Control of the width of active Western Antarctic Siple Coast ice streams by internal melting at their margins

Thibaut Perol[1] and James R. Rice[1,2]
Submitted to J. Geophy. Res. Earth Surf. on 2 June, 2014

Abstract. We examine, and find evidence to support, the hypothesis that the width of Siple Coast ice streams in West Antarctica is set by the development of significant internal melting (i.e., development of temperate ice conditions) within the ice sheet at the margins. We first illustrate, from published ice sheet deformation data and from simple 1-D thermal modeling based on temperature-dependent flow and conduction properties, that most existing Siple Coast ice stream margins are in a state of partial melt, with temperate ice being present over a substantial fraction of the sheet thickness. We show that, although the margins sustain high lateral strain rates, they can support (and hence transmit to the cold ridges) notably less lateral shear stress than would the somewhat less rapidly deforming ice located inboard, away from the ridge. We then propose, and quantify approximately, a possible related mechanism of margin formation, that is, of locking the sheet to the bed at the margin. Shear heating of the temperate ice continually generates melt, which percolates toward the bed below. If this develops a channelized marginal drainage of Röthlisberger type, the standard theory argues that the high, nearly lithostatic, basal pore pressure elsewhere (i.e., near the bed within the fast moving stream) is somewhat alleviated within the channel. This results in a higher Terzaghi effective normal stress, which we quantify approximately, acting along the bed near the channel, thereby creating high resistance against frictional shear and possibly locking the ice to the bed, naturally forming an ice stream margin. Our estimates are that the effective normal stress acting on the bed just outside such a channel, and hence the till shear strength, can be twenty to sixty times larger than that inferred to be present at the bed within the fast-moving stream. Reduced basal fluid pressure, and hence enhanced strength, over a broad region near the margin is shown sufficient to remove the strong stress concentration at the slipping to locked bed transition, and provides a stabilizing mechanism for the margin.

1. Introduction

A complete collapse of the West Antarctic ice sheet would raise the global sea level by approximately three to five meters [*Bamber et al.*, 2009; *Vaughan and Spouge*, 2002]. Siple Coast ice streams (SCIS) in West Antarctica drain a large amount of ice into the Ross Ice Shelf at speeds of hundreds of m.yr^{-1}, which is approximately two to three orders of magnitude higher than for the surrounding ice [*Shabtaie and Bentley*, 1987]. The evidence of recent and rapid changes of stream flow rates within a few decades [*Joughin et al.*, 2005] may have a significant effect on the sea level over time scales of centuries. Because the width of the rapid flowing ice may control the net mass flow rate [*Van Der Veen and Whillans*, 1996], we worked on identifying mechanisms that could set the location, or at least greatly slow the expansion, of the stream margins.

The SCIS are about 1 km thick, active along hundreds of kilometers, are typically 30 to 80 km wide and have low surface slopes ($\sim 1.3 \times 10^{-3}$) [*Joughin et al.*, 2002]. The ice flow is driven by a relatively small gravitational driving stress ($\sim$

10 kPa), thought to be accommodated primarily through basal drag and laterally shear stressed zones at the margins [*Whillans and Van Der Veen*, 1993]. However, they are underlain everywhere by a Coulomb-plastic bed with an extremely low yield strength ($\sim$ 1 to 5 kPa) [*Kamb*, 2001] due to a pore pressure in the bed sediments that is nearly equal to the ice overburden pressure. Hence, most of the resistance to the driving stress is provided by side drag [*Joughin et al.*, 2004a], itself provided because of elevated basal shear stress just outside the shear margins where the till is frozen [*Raymond et al.*, 2001].

Over the past two decades, numerous studies intended to quantify in which proportion side drag supports the downslope weight of ice streams. Detailed analysis of transverse velocity profiles across streams using analytical and numerical models of ice flow have shown that ice cannot have uniform properties across the ice stream. At margins where the shear strain rate is high, the ice should be warmer and thus weaker than in the central part of the stream (e.g., *Echelmeyer et al.* [1994] for Whillans ice stream (Whillans IS) and *Scambos et al.* [1994] for Bindschadler ice stream (Bindschadler IS)). Using the shear strain rate profile, a stress-equilibrium in the downstream direction, ignoring the longitudinal force gradient, and considering the lateral shear strain rate as uniform over depth, they attempted to adjust the distribution of basal drag across the stream to keep it positive. This was found to not be possible when the temperature-dependent creep parameter A of Glen's law, $\dot{\epsilon}_{ij} = A\tau_E^2\tau_{ij}$ [*Cuffey and Paterson*, 2010], is assumed to be laterally homogeneous. Both *Scambos et al.* [1994], who allow A to vary with depth according to an input temperature

---

[1]School of Engineering and Applied Sciences, Harvard University, Cambridge, Massachusetts, USA.

[2]Department of Earth and Planetary Sciences, Harvard University, Cambridge, Massachusetts, USA.

profile, and *Echelmeyer et al.* [1994], who set A to be vertically uniform at its value for -15 °C, are able to fit the strain rate profile only by introducing an enhancement factor E in Glen's law ($\dot{\epsilon}_{ij} = EA\tau_E^2\tau_{ij}$) that varies laterally. This factor illustrates lateral softening close to the margins due to such factors as shear heating or oriented ice fabric developed by a large accumulation of shear strain. Since *Jackson and Kamb* [1997] have sampled the ice where *Echelmeyer et al.* [1994] invoke large softening, and have not found a strongly developed single maximum fabric that would be expected in such a shear zone (a fabric with c-axis oriented normal to the lateral shear plane), we explore the role of shear heating on the mechanism of margin weakening.

In this paper, we use a simplified 1-D conduction-advection heat transfer analysis that predicts the vertical distribution of temperature at the SCIS margins. Its limitations are explored in *Suckale et al.* [2014], in which it is found to produce qualitatively credible estimates. We incorporate the internal shear heating from lateral deformation of ice at the margins, neglected in the previously mentioned studies, and temperature-dependence of the flow and conduction properties in the heat equation. However this model is too simple to accommodate horizontal advection of ice from/to the ridge.

From published ice sheet deformation data [*Joughin et al.*, 2002] and simple thermal modeling, we find here that most margins are in a state of partial melt with temperate ice present over a substantial fraction of the sheet thickness adjoining the bed. This concept agrees with previous modeling studies of strain heating in a single theoretical shear margin [*Jacobson and Raymond*, 1998; *Schoof*, 2012; *Suckale et al.*, 2014], which suggest that a core of temperate ice can extend vertically as much as several hundred meters.

Shear heating of temperate ice continually generates meltwater at ice grain interfaces, which percolates toward the bed below via a vein and node system described by *Nye* [1989] in polycrystalline ice. From a measured shear strain rate profile across the southern margin of Whillans ice stream B2 (Whillans IS B2) [*Echelmeyer and Harrison*, 1999], we predict the extension of the temperate zone in 2-D, relying on the severe assumptions that we can neglect horizontal diffusion and advection. These assumptions are discussed and results are compared to more elaborate thermal modeling developed in *Suckale et al.* [2014]. Equating the shear heating to the latent heat in the temperate zone, we quantify the meltwater supply along the bed and suggest that it could cause the development of a marginal channelized drainage of Röthlisberger type. Standard theory argues that the high, nearly lithostatic, pore pressure near the bed within the fast moving stream is somewhat alleviated within the channel, which operates at reduced water pressure [*Röthlisberger*, 1972; *Nye*, 1976] relative to the ice overburden pressure. This results in a higher Terzaghi effective stress just outboard of the channel, which plausibly locks the ice to the bed, naturally forming a limit to the width of the stream of fast-flowing ice. This paper examines the hypothesis that internal melting at margins could control the width of active SCIS by locking or, at least, slowing the migration of the margins.

2. Model of partially melted margins: thickness of temperate ice

SCIS margins are subjected to internal heat production from straining, especially from lateral shear deformation of the ice. We first incorporate the ice deformation-heating work in a standard 1-D vertical heat transfer analysis and find evidence of internal melting at the margins. We, thus, solve a 1-D model with a full temperature dependence of

ice properties, allowing for a temperate zone when the shear strain rate is sufficient. We find that eleven of the sixteen SCIS margins sampled by *Joughin et al.* [2002] are at or very close to a strain rate level sufficient to partially melt the ice sheet. This put them in a weakened state such that they deform faster but carry the same thickness-averaged lateral shear stress. That is because the relation between the lateral shear strain rate (assumed uniform over depth in the 1-D model) and lateral shear stress is shown to be triple-valued. This would allow the margins to strain faster than the ice to either side of the margin if subjected to the same thickness average lateral shear stress. In fact, we present evidence that the margins are supporting less lateral stress than adjacent ice of the more rapidly moving stream. Such requires that basal resistance be enhanced near the margin, and we show such enhancement to be a standard consequence of a channelized drainage of meltwater. Hence, we argue that internal melting within the ice sheet is, perhaps, related to why margins are where they are.

2.1. Evidence of internal melting at SCIS margins

Let us consider an ice stream cross section as depicted in Figure 1. The ice stream is flowing in the downstream direction x, y is transverse to the flow and positive outward from the stream center, and z is the vertical coordinate taking a positive upward direction from the base of the ice (the notations used in this paper are reported in the Notation section). Let (u, v, w) be the velocity components associated to the (x, y, z) coordinates. Let us define, respectively, the lateral shear stress on lateral planes through the ice sheet oriented parallel to the flow and the basal shear stress as $\tau_{lat} = -\tau_{xy}$ (where $y > 0$) and $\tau_{base} = -\tau_{xz}$. This ice stream is driven by a gravitational driving stress, a force per unit base area, $\tau_{grav} = \rho_{ice}gHS$ where ρ_{ice} is the ice density, g the acceleration due to gravity, H is the ice sheet
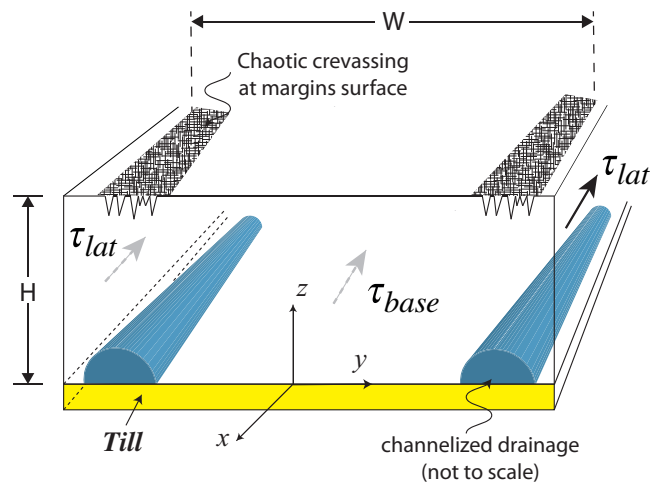
Figure 1. Sketch of a SCIS cross section. Ice thickness H greatly exaggerated relative to stream width W; typically $W/H \sim 30$ to 85 for ice streams and ~ 10 to 20 for their tributaries. The ice is flowing on a low-permeability soft bed called till (in yellow). Chaotic crevassing is observed at the surface of the margins [*Harrison et al.*, 1998; *Echelmeyer and Harrison*, 1999]. Given the evidence we develop for internal melting, we hypothesize that a channelized drainage (in blue) exists at the margins along the bed and collects the water produced within the ice sheet above. The channel diameter grows with distance downstream.
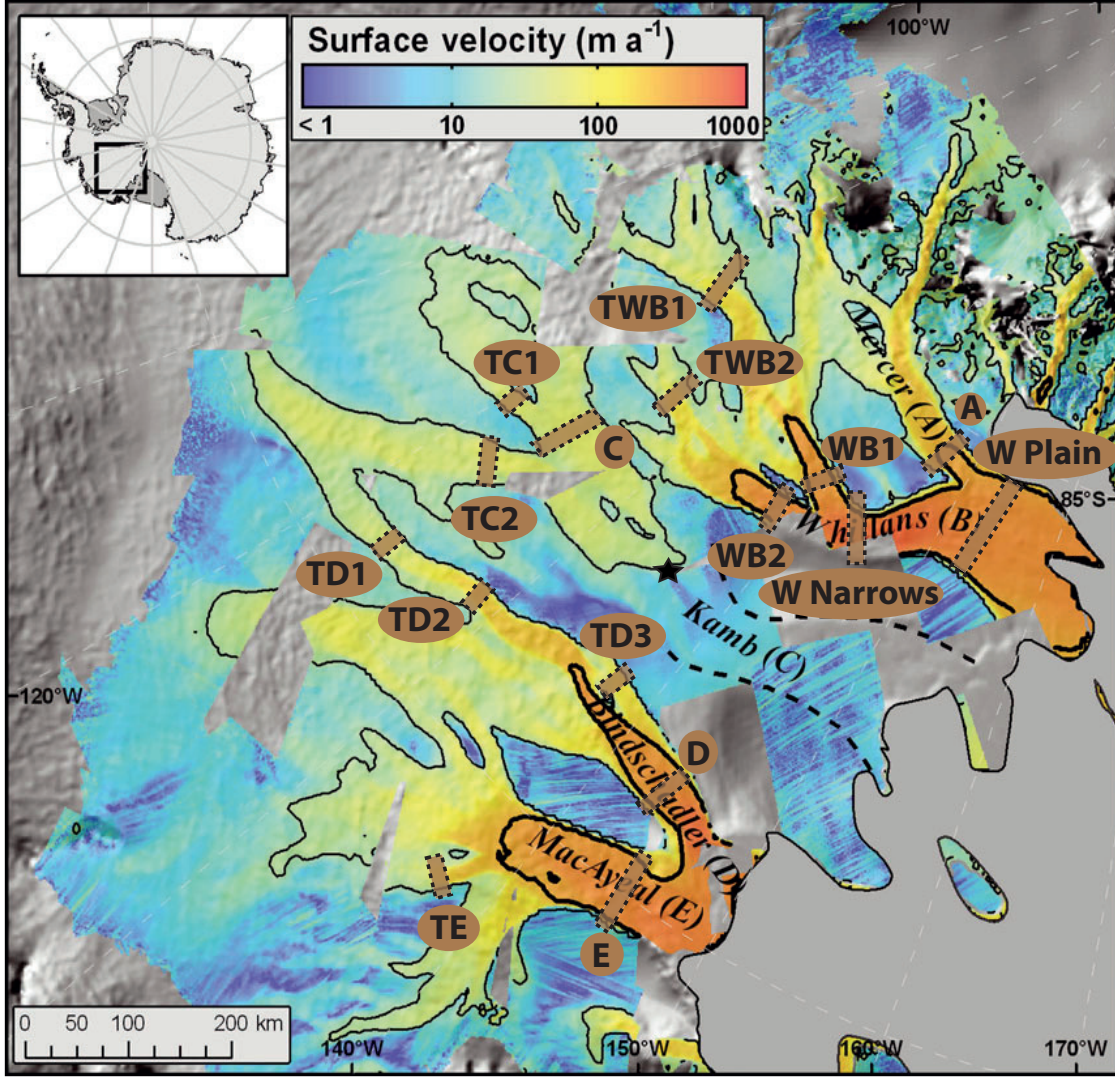
Figure 2. Surface velocity of SCIS, modified from *Le Brocq et al.* [2009]. Velocity contours shown are 25 m.yr^{-1} (thin line) and 250 m.yr^{-1} (thick line). *Joughin et al.* [2002] made profiles represented by brown lines and named in the brown circles or ovals to extract the parameters reported in Table 1. Profiles beginning with the letter T are made at the tributaries of ice streams, before the onset of streaming flow. The black star indicates the location of a borehole made at one shear margin of Kamb IS by *Vogel et al.* [2005].

thickness and S the absolute value of the surface slope that measures the inclination of the slab. A simple force balance at a distance y from the center of an ice stream, that considers a laterally constant thickness H, and neglects any variation in net axial force in the sheet [*Whillans and Van der Veen*, 1997], shows that the thickness-averaged $\bar{\tau}_{lat} = \bar{\tau}_{lat}(y)$ increases with distance y from the center, scaling with the difference between the average over the width y gravitational stress and the average over the width y basal resistive stress $\bar{\tau}_{base}$ as,

$$\tau_{lat}(y)H = (\tau_{grav} - \bar{\tau}_{base})\,y. \tag{1}$$

The lateral strain rate transverse to the downslope direction and predicted by Glen's law ($\dot{\gamma}_{lat} = 2A\tau_{lat}^3$ where the "engineering" shear strain rate is $\dot{\gamma}_{lat} = -2\dot{\epsilon}_{xy}$ where $y > 0$) increases as τ_{lat}^3. Then, the heating work rate $\bar{\tau}_{lat}\dot{\gamma}_{lat}$ associated with the lateral deformation of ice increases as $\bar{\tau}_{lat}^4$, hence, roughly proportionally to y^4. It quickly becomes a significant heat source within the ice sheet with increasing width, and must ultimately induce internal melting at a large enough distance from the center of the stream, if

some process does not limit stream expansion. That is why we later introduce the shear heating in a thermal model of well-developed margins.

The energy equation governing heat transfer and temperature T within an ice sheet, is

$$\Phi - \vec{\nabla} \cdot \vec{q} = \rho_{ice}C_i\left(\frac{\partial T}{\partial t} + \left(\vec{v} \cdot \vec{\nabla}\right)T\right), \tag{2}$$

where Φ is the volumetric rate of stress working, $\vec{q} = -K\vec{\nabla}T$ the heat flux vector, K is the thermal conductivity, ρ_{ice} the ice density, C_i the ice specific heat, t the time, and $\vec{v}$ the ice velocity vector. Rewriting in a 1-D approximation, $T = T(z,t)$, the previous equation now gives the equation governing the vertical temperature distribution of an ice column and it reduces at steady state, $T = T(z)$, to

$$\frac{d}{dz}\left(K\frac{dT}{dz}\right) - \rho_{ice}C_iw\frac{dT}{dz} + \Phi = 0, \tag{3}$$

where w is the vertical (z direction) component of $\vec{v}$.

2.2. Simplified thermal model- Analytical solution to the 1D heat conduction-advection model with internal melting

In this subsection we use temperature-independent ice properties to provide an analytical solution of the 1D temperature profile with internal melting due to stress working. This solution allows, in regions in which the ice straining is significant, more accurate calculations of the average over the ice sheet thickness creep parameter sometimes used in numerical models based on *Zotikov* [1986]'s vertical temperature distribution. The paper is written such that this subsection can be omitted and the reader interested in our 1D numerical model of temperate margins using full temperature dependence of ice properties and used in the rest of the paper can skip to subsection 2.3.

There are only a few measured temperature profiles with depth (especially at shear margins where access conditions are dangerous) [*Harrison et al.*, 1998], and because it allows finding an analytical solution for a specific velocity profile and an internal heating rate constant over depth, we first consider all temperature dependent parameters (K, C_i and the creep parameter A) as constant (a restriction that is lifted in the next subsection), evaluating them at an average temperature $T_{avg} = H^{-1} \int_0^H T(z)\mathrm{d}z$ approximated as $T_{avg} = (T_{atm} + T_{melt})/2$. For this the constant thermal diffusivity becomes $\alpha_{th} = K/\rho_{ice}C_i$.

At a margin, the lateral deformation of ice induces a significant work rate, $\Phi = \tau_{lat}\dot{\gamma}_{lat}$ (neglecting the heating from other stress components). Here, we adopt a simple model based on the approximation, as in *Echelmeyer et al.* [1994] and *Scambos et al.* [1994], in which the lateral shear strain rate is uniform over depth (which of course becomes questionable where the sheet is frozen to the bed). Therefore, the lateral shear stress, estimated using Glen's law,

$$\tau_{lat} = A_{avg}^{-1/3}(\dot{\gamma}_{lat}/2)^{1/3}, \qquad (4)$$

is also treated as uniform over depth ($A_{avg} \equiv A(T_{avg})$).

We assume a melting rate at the base $v_m \equiv -w(z = 0)$, we neglect $\partial v/\partial y$ and take the downslope stretching rate $\partial u/\partial x$ as a constant, written as a/H. Then the ice incompressibility constraint implies,

$$w(z) = -v_m - \frac{az}{H}, \qquad (5)$$

and the surface accumulation rate in the uniform H approximation is, therefore, $a + v_m$. As commonly denoted in the literature, we refer to a as the "accumulation rate".

Margin temperatures are sensitive to the transverse influx of colder ice from the ridge zone [*Jacobson and Raymond*, 1998; *Suckale et al.*, 2014] and, more importantly, to the margin migration rate which may be of order of 10 m.yr^{-1}, an order of magnitude higher than the transverse motion of ice into the margin [*Harrison et al.*, 1998; *Echelmeyer and Harrison*, 1999; *Schoof*, 2012]. However, evidence for margin migration is not found at all SCIS. Given the limited study and the lack of any suitable method of including these effects in our 1-D modeling, we intentionally neglect these terms in the 1-D heat analysis and discuss their possible thermal effect later (cf. Discussion section). Therefore, our 1-D vertical heat transfer analysis that considers diffusion, vertical (only) advection and internal shear heating becomes,

$$\alpha_{th}\frac{\mathrm{d}^2T}{\mathrm{d}z^2} + \left(\frac{az}{H} + v_m\right)\frac{\mathrm{d}T}{\mathrm{d}z} + \frac{\tau_{lat}\dot{\gamma}_{lat}}{\rho_{ice}C_i} = 0. \qquad (6)$$

This gives the temperature profile of a column of ice at the margin assuming a bed temperature at the pressure-dependent melting point,

$$T_{melt} = 273.15 \text{ K} - \frac{7.4 \times 10^{-8} \text{ K}}{\text{Pa}}\rho_{ice}gH \qquad (7)$$

following *Hooke* [2005] (water is present at the ice-till interface [*Vogel*, 2004; *Vogel et al.*, 2005]), and a representative annual average atmospheric temperature T_{atm} at the surface. This analysis deviates from the commonly used *Zotikov* [1986] steady state model in incorporating the shear heating term and a basal melting rate.

Using $T_{atm} = -26$ °C, $A_{avg}^{-1/3} \sim 521$ kPa.yr$^{1/3}$ [*Cuffey and Paterson*, 2010], a surface accumulation rate range from $a = 0.1$ m.yr^{-1} to $a = 0.2$ m.yr^{-1} [*Giovinetto and Zwally*, 2000; *Spikes et al.*, 2004], a basal melting rate range up to $v_m = 20$ mm.yr^{-1} [*Joughin et al.*, 2004b; *Beem et al.*, 2010], and an ice thickness and shear strain rate as measured at Mercer ice stream margin (Profile A in Figure 2) and reported in Table 1, we find that, because of the shear heating, we predict temperatures in excess of the melting temperature over a substantial fraction of the ice sheet thickness
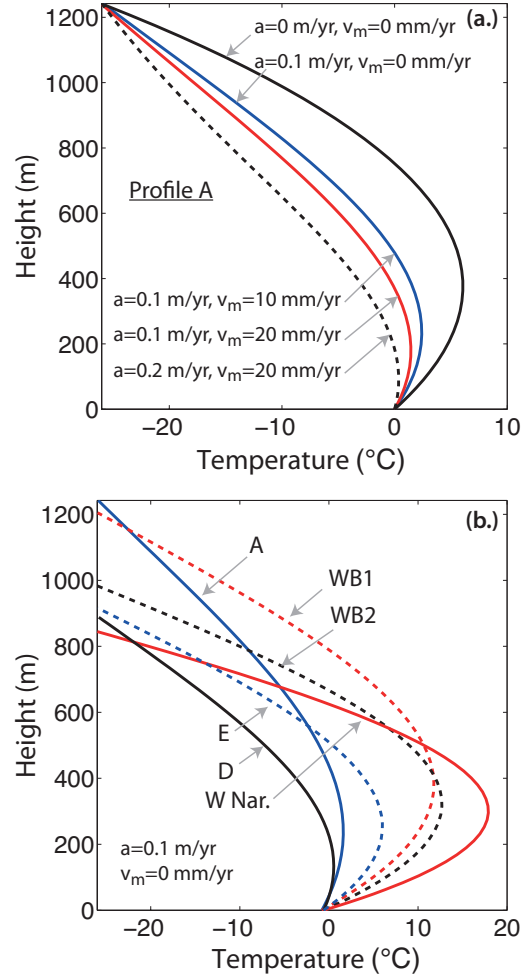
Figure 3. Temperature solution of the 1-D diffusion-advection model with shear heating as an internal heat source written in equation (6), a thermal diffusivity α_{th} of 1.3×10^{-6} m^2.s^{-1}(a.) Ice sheet thickness, strain rate and melting temperature are taken from the margin of Mercer ice stream (Table 1). Basal temperature gradient is positive for the three advection profiles used. (b.) Temperature profiles at margins of Mercer (A), Whilans (WB1, WB2 and W Nar.), Bindschadler (D) and MacAyeal (E) with $a = 0.1$ m.yr^{-1}, $v_m = 0$ m.yr^{-1} and H, T_{melt} and $\dot{\gamma}_{lat}$ given in Table 1. The calculated basal temperature gradient is positive for the six profiles; thus, $T > T_{melt}$ is (unrealistically) predicted, implying that a zone of temperate ice must exist.

(Figure 3a). If the linear vertical velocity profile is valid at the margins, numerical solutions show that the downward motion of cold ice at a rate of $a + v_m$ at the top and v_m at the bottom cools the ice column. In addition, this basal melt rate may vary rapidly as we move toward the ridge and is poorly constrained at margins; thus, we choose to ignore v_m in equation (6). For $v_m = 0$, we find the analytical solution of equation (6) which matches the boundary conditions $T(z = 0) = T_{melt}$ and $T(z = H) = T_{atm}$ (cf. appendix A),

$$
\begin{aligned}
T(z) \ &= T_{melt} + (T_{atm} - T_{melt}) \frac{\mathrm{erf}\left(\sqrt{\mathrm{Pe}/2}\,(z/H)\right)}{\mathrm{erf}\left(\sqrt{\mathrm{Pe}/2}\right)} \\
&- \frac{\tau_{lat}\dot{\gamma}_{lat}H^2}{K_{avg}\mathrm{Pe}}\left[\int_0^1 \frac{1 - \exp\left(-\lambda\mathrm{Pe}z^2/2H^2\right)}{2\lambda\sqrt{1-\lambda}}\,\mathrm{d}\lambda \right. \\
&\left. - \frac{\mathrm{erf}\left(\sqrt{\mathrm{Pe}/2}\,(z/H)\right)}{\mathrm{erf}\left(\sqrt{\mathrm{Pe}/2}\right)}\int_0^1 \frac{1 - \exp\left(-\lambda\mathrm{Pe}/2\right)}{2\lambda\sqrt{1-\lambda}}\,\mathrm{d}\lambda\right],
\end{aligned} \quad (8)
$$

with the Péclet number $\mathrm{Pe} = aH/\alpha_{th}$. When we neglect the shear heating product $\tau_{lat}\dot{\gamma}_{lat}$, this reduces to the solution already found by *Zotikov* [1986].

For a set of six active ice stream profiles (A, WB1, WB2, W Narrows, D, E) located in Figure 2 and running across, respectively, Mercer, Whillans, Bindschadler and MacAyeal ice streams, the lower part of the temperature profile at the margins predicted by relation (8) shows temperatures in excess of the melting point (cf. Figure 3b), using a sensible value of 0.1 m.yr^1 for the accumulation rate [*Giovinetto and Zwally*, 2000; *Spikes et al.*, 2004]. Ultimately, we presume that the ice sheet at SCIS margins is temperate over some depth range, hence, supporting the possibility that internal melting within the ice sheet is related to why the active margins are where they are.

2.3. Model set up, allowing for temperate zone and full temperature dependence of ice properties

Since the ice temperature could not be greater than T_{melt} as the previous simplified model predicted, we next solved

a 1-D diffusion-advection heat transfer analysis allowing for local internal melting and a temperature capped at the melting point, such that a height H' of ice, adjoining the bed, is temperate like in Figure 4. The lateral shear strain rate, $\dot{\gamma}_{lat}$, is again taken uniform through the ice thickness. τ_{lat} is now the local shear stress on lateral planes through the ice sheet oriented parallel to the flow. It is directly related to the temperature profile via the creep law since the creep parameter A is temperature dependent. Consequently, the local volumetric rate of internal heat production is

$$
\tau_{lat}(T)\dot{\gamma}_{lat} = 2A(T)^{-1/3}\left(\frac{\dot{\gamma}_{lat}}{2}\right)^{4/3} \quad (9)
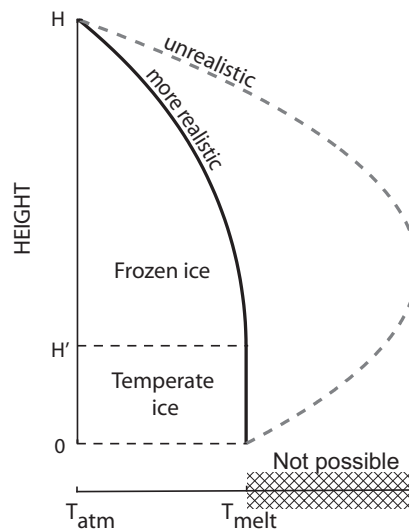$$

The temperature dependence of the creep parameter is treated explicitly using the function proposed by *Cuffey and Paterson* [2010] (page 72), which fits results from field analyses and laboratory experiments.

$$
A(T) = A^* \exp\left(-\frac{Q_c}{R}\left[\frac{1}{T_h} - \frac{1}{T^*}\right]\right) \quad (10)
$$

The pre-exponential constant is 3.5×10^{-25} s^{-1}.Pa^{-3} and the melting temperature corrected from pressure dependence is $T_h = T + c_p P$ with $c_p = 7 \times 10^{-8}$ K.Pa^{-1}, T in Kelvin and activation energy $Q = 60$ kJ.mol^{-1} for $T_h < T^*$ and $Q = 115$ kJ.mol^{-1} when $T_h < T^*$ with $T^* = -10°$C. Thermal conductivity K and specific heat C_i of ice are also allowed to vary with respect to temperature. Following the discussion on the forms of the dependence of these two latter parameters on T, in Kelvin (K), by *Cuffey and Paterson* [2010] (page 400), we use

$$
K(T) = 9.828 \ \frac{\mathrm{W}}{\mathrm{m.K}} \ \exp(-5.7 \times 10^{-3} \ \frac{T}{\mathrm{K}}) \quad (11)
$$

$$
C_i = \left(152.5 + 7.122 \ \frac{T}{\mathrm{K}}\right) \ \frac{\mathrm{J}}{\mathrm{kg.K}} \quad (12)
$$

Table 1. Parameters taken from *Joughin et al.* [2002] and used for margins of the profiles located in Figure 2. Profiles beginning with the letter T are made at the tributaries of the ice streams.

Ice Stream	Profile	H (m)	W (km)	$\dot{\gamma}_{lat}$ (10^{-2}.yr^{-1})
Mercer	A	1242	39	4.2
Whillans	WB1	1205	35	7.0
	WB2	985	34	9.5
	W Narrows	846	48	13.5
	W Plain	735	121	5.1
	TWB1	2188	25	3.8
	TWB2	1538	25	4.0
Kamb	C	1805	69	1.0
	TC1	1802	17	1.4
	TC2	2196	43	0.9
Bindschadler	D	888	55	5.8
	TD1	1952	24	2.5
	TD2	1412	35	5.4
	TD3	1126	21	2.2
MacAyeal	E	916	78	8.1
	TE	1177	19	5.5

Figure 4. Sketch of the 1-D thermal model of a partially melted margin of SCIS. A height H' is at the melting point taken to be the pressure-melting point at the bed and uniform over depth, so that there is no vertical heat conduction in this lower layer. The temperature in the rest of the ice sheet (frozen ice upper part) is predicted by a 1-D diffusion-advection heat transfer analysis with internal heating due to ice deformation.

The governing equation of our more refined, but still 1-D model, is now

$$\frac{\mathrm{d}}{\mathrm{d}z}\left(K(T)\frac{\mathrm{d}T}{\mathrm{d}z}\right) + \rho_{ice}C_i(T)\frac{az}{H}\frac{\mathrm{d}T}{\mathrm{d}z} + 2A(T)^{-1/3}\left(\frac{\dot{\gamma}_{lat}}{2}\right)^{4/3} = 0$$

$$(13)$$

T in the upper part of the ice sheet, where the ice is frozen, and H', the height of temperate ice adjoining the bed, are the unknowns (cf. Figure 4). Mathematically, this takes the form of a free boundary problem in 1-D. The equation is solved subject to boundary conditions $T(z = H) = T_{atm}$, $T(z = H') = T_{melt}$ and $\mathrm{d}T/\mathrm{d}z$=0 at $z = H'$. We set T_{melt} to be uniform over depth and at its temperature for a pressure equal to the overburden pressure at the bed using equation (7).

When the level of strain rate is enough to melt the ice sheet, we allow some lower depth range to be partially melted at $T = T_{melt}$ and the rest of the temperature profile is predicted by equation (13). Therefore, the solution of this model, found numerically by standard Runge-Kutta procedures and shooting techniques, gives the proportion of the ice sheet that is temperate depending on the ice sheet thickness and the shear strain rate imposed. For all the ice streams we set $T_{atm} = -26\ °C$ and the surface accumulation rate a at 0.1 m.yr^{-1}, a reasonable estimate according to *Giovinetto and Zwally* [2000] and *Spikes et al.* [2004].

2.4. What fraction of the ice thickness is temperate at the margins?

Sixteen ice stream transverses (across the flow) downslope velocity profiles have been reported by *Joughin et al.* [2002]; see locations in Figure 2. For each profile they provide in their Table 3 and 4 the ice sheet thickness extracted from a Digital Elevation Model [*Lythe and Vaughan*, 2001], the width taken to be the distance between the two peaks in the transverse profile of lateral shear strain rate, an average lateral drag calculated via a force balance and an average creep parameter over the entire ice sheet thickness assuming a temperature distribution as in our equation (8) with $\dot{\gamma}_{lat} = 0$ to perform force balance calculations. Assuming a strain rate of equal magnitude at both margins of all profiles they reported, and using their equations (1) and (3), we invert the strain rates they measured at the margins. We use these values of shear strain rate $\dot{\gamma}_{lat}$ at margins, ice stream width W and ice thickness H, reported in Table 1, for our thermal modeling. These lateral strain rate values inferred from downstream velocity profiles are decreased by the 3.5 km smoothing filter used to reduce the noise. Significant variations in strain rates occurring over distances lower than 2 km, as typically observed at shear margins [*Scambos et al.*, 1994; *Echelmeyer and Harrison*, 1999], are not captured. Therefore we may expect actual values of strain rate peaks at margins higher than the ones displayed in Table 1. In addition to these data, *Scambos et al.* [1994] have made a series of ice-speed profiles and found that the maximum ice speed and strain rate at the southern margin of Bindschadler IS increases dramatically from 420 to 670 m.yr^{-1} and 0.02 to 0.16 yr^{-1} as the margin develops along 55 km in the downstream direction. Consequently, the results presented in that section and predicted by our 1-D model of temperate margins are valid for the particular downstream location considered (i.e., for the specific ice sheet thickness and strain rate value reported in Table 1).

Our analysis predicts that, of the seven profiles made on active SCIS (this excludes Kamb IS), six margins are at a level of strain rate at which internal melting occurs or is close to taking place. Respectively, 9, 39, 38, 45, and 26% of the ice thickness of Mercer, Whillans B1, Whillans B2, Whillans and MacAyeal ice stream margins are predicted to be temperate (see ratio H'/H in Table 2). The strain rate level measured at Bindschadler IS (0.058 yr^{-1} at margins of profile D) is not enough to melt a portion of the 888 m ice thickness, although the onset of melting (i.e., $H'/H = 0^+$), would be predicted for a 5% increase to 0.061 yr^{-1}. In fact using the standard deviation provided by *Joughin et al.* [2002], the maximum value of strain rate in their error bar would be enough to melt 7 % of the ice sheet. Also, as one moves approximately 30 km downstream, the maximum strain rate observed at the Bindschadler stream southern margin increases far in excess of that, by $\sim 280\%$ and reaches 0.16 yr^{-1} [*Scambos et al.*, 1994], as noted. For a comparable ice thickness to what has been measured at profile D, that level of strain rate would melt 53% of the ice sheet thickness according to our model. The margins of W Plain profile, made further downstream than any other profile on Whillans IS, are not predicted to be temperate. However, at this location the IS becomes flatter and wider; its characteristics are quite different than the other SCIS.

Our studies also predict that five of the six margins of the tributaries of the active SCIS (again Kamb IS is excluded) are also in a state of partial melt, with temperate ice being present over a fraction of the ice sheet adjoining the bed. The fractions of the marginal ice sheet thickness of profiles TE, TD1, TD2, TWB1 and TWB2, respectively, made at the tributaries of MacAyeal, Bindschadler, Whillans B1, and Whillans B2 that are predicted to be temperate are respectively, 23, 16, 37, 50, and 26%. However, profiles made at the active upper part of Kamb IS are not predicted to have marginal temperate ice. There, the ice flow does not have the characteristics of streaming flow (e.g., almost twice the thickness of other streams and a low marginal strain rate, less than 0.01 yr^{-1}).

We conducted a sensitivity analysis of the model exploring the results for a vanishing ice vertical advection (that is if the downslope stretching matches the transverse compression of ice at the margins), and for a doubled accumulation rate, $a = 0.2$ m.yr^{-1}, as it was shown to be variable both in time and space by *Giovinetto and Zwally* [2000] and *Spikes et al.* [2004]. Without vertical advection, we found that 22, 42, 42, 46, 11, and 32 %, respectively, of the ice height of Mercer, Whillans B1, Whillans B2, Whillans, Bindschadler and MacAyeal ice stream margins are temperate. For a high accumulation rate of 0.2 m.yr^{-1}, 31, 33, 41, and 15 %, respectively, of the ice height of Whillans B1, Whillans B2, Whillans, and MacAyeal ice stream margins are found to be temperate.

2.5. Ice stream force partitioning that considers temperate ice at margins

Since we emphasize having a more accurate temperature profile at the margins, we evaluate the side drag to quantify the force partitioning i.e., to what degree is the gravitational driving stress balanced by basal shear stress and lateral drag assuming insignificant gradient in axial force.

The average lateral shear stress $\bar{\tau}_{lat}$ over the ice sheet thickness, neglecting any porosity effect on strength in the temperate region, is calculated for each temperature profile with,

$$\bar{\tau}_{lat} = \frac{1}{H}\int_0^H A(T)^{-1/3}\mathrm{d}z\left(\frac{\dot{\gamma}_{lat}}{2}\right)^{1/3}.\qquad (14)$$

Lateral stresses are reported in Table 2. Because we allow a height H', adjoining the bed, to be temperate, $\bar{\tau}_{lat}$ predicted by equation (14) is lower than the lateral shear stress estimated by *Joughin et al.* [2002] for frozen margins of similar thickness.
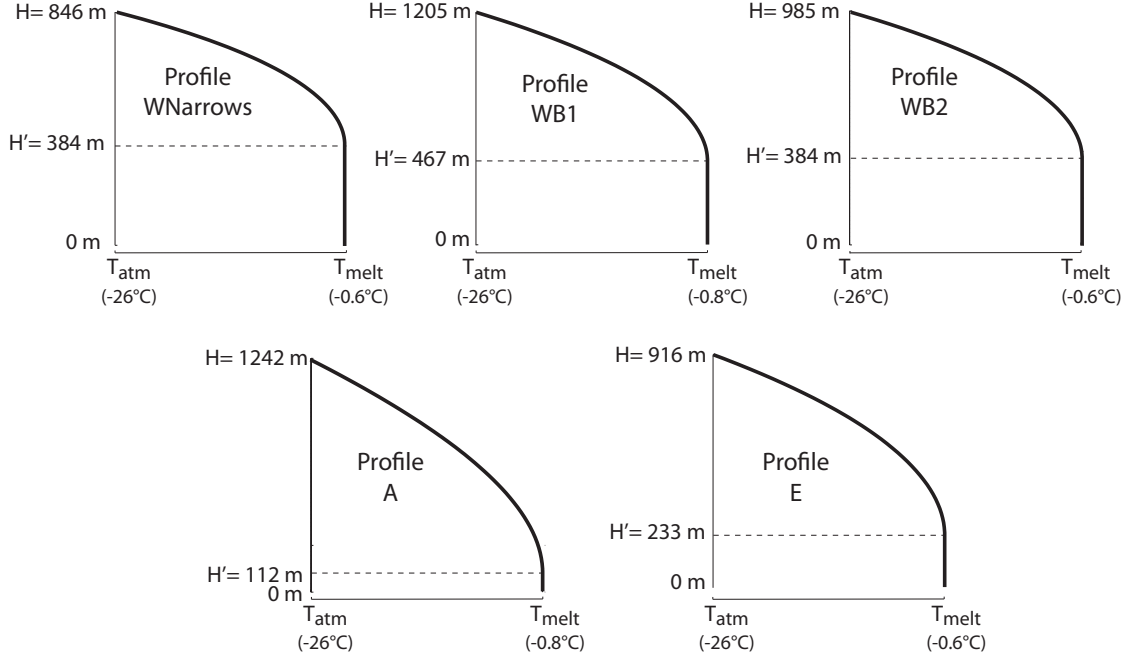
Figure 5. Temperature profile predicted by the 1-D thermal model of margins of profiles located in Figure 2 for an ice sheet thickness and a lateral strain rate as reported in Table 1. The strain rate level measured at Bindschadler IS (0.058 yr^{-1}) is insufficient to melt a portion of the 888 m ice thickness.

A simplified force balance of an ice stream that neglects any variation in net axial force in the sheet (shown to be accurate for Whillans IS [*Whillans and Van Der Veen*, 1993]) and transverse variation of ice thickness, gives us the average basal shear stress $\bar{\tau}_{base}$ over the width for each profile studied,

$$\bar{\tau}_{base} = \tau_{grav} - \frac{2\bar{\tau}_{lat}H}{W} \qquad (15)$$

Using this latter relationship and Table 1, we find values of basal drag, reported in Table 2, of the order of 3 to 12 kPa under the active SCIS, clearly indicative of a weak bed underlying the ice.

On Whillans IS B1 and B2 $\bar{\tau}_{base}$ is estimated at 5.0 and 3.6 kPa. These values are higher than in-situ shear strength measurements of basal till (*Kamb* [2001] found a strength of 2 kPa near Up B, a camp at Whillans B2 IS located on the map in Figure 6), and the range of 1.2 to 2.8 kPa found by *Joughin et al.* [2003], who used control method inversion of a high-resolution velocity data set to find the basal shear stress corresponding to a plastic bed. However, when they do consider an enhancement factor (E=3) that models the margins weakening due to shear heating, their values are slightly larger than ours (5.8 and 5.3 kPa for B1 and B2). Consequently, even with a model that allows a height of the ice at margins to be temperate and ultimately treats the margin weakening expected there, the till under Whillans IS is inferred to be very weak. Additionally, we find that where Whillans stream is about 35 to 50 km wide (before the ice plain and at the two tributaries B1 and B2), the bed supports only around 35% of the gravitational driving stress (Table 2). More measurements in the downstream direction from the tributaries to the ice plain could show if we recognize here a special feature of this stream. Still, at tributaries of Whillans IS, basal drag is moderate (about 30 kPa) and

provides more resistance to the larger driving stress ($\sim$ 68 %).
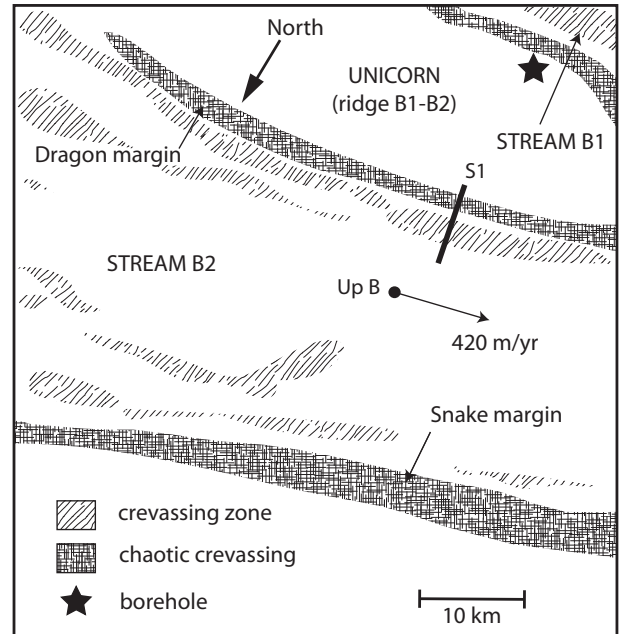
Figure 6. Location of profile S1 on Whillans IS B2 (see Figure 2) where *Echelmeyer et al.* [1994] measured a surface velocity profile to extract the Dragon margin shear strain rate profile. The black star at the interstream ridge between Whillans IS B1 and B2, an area commonly referred to as the Unicorn, indicates the location of a borehole made by a Caltech group (mentioned in a personal communication from H. Engelhardt by *Clarke et al.* [2000]). At Up B, the ice velocity is measured at 420 m.yr^{-1}. North-South axis is approximately perpendicular to Dragon margin. (redrawn and modified, based on *Echelmeyer and Harrison* [1999]).

Table 2. Ice streams and their tributaries gravitational driving stress as measured at profiles located in Figure 2 and calculated temperate ice height fraction, lateral stress, basal shear stress, and ratio of basal stress to driving stress, neglecting the gradient in net axial force. Profiles beginning with the letter T are made at the tributaries.

Ice Stream	Profile	τ_{grav}[a](kPa)	H'/H (%)	$\bar{\tau}_{lat}$ (kPa)	$\bar{\tau}_{base}$ (kPa)	$\bar{\tau}_{base}/\tau_{grav}$ (%)
Mercer	A	14.9	9	112.3	7.7	52
Whillans	WB1	12.5	39	113.4	5.0	38
	WB2	10.8	39	124.2	3.6	33
	W Narrows	7.6	45	135.0	2.8	37
	W Plain	3	0	97.0	1.8	61
	TWB1	47.5	50	89.0	32.0	67
	TWB2	40.9	26	101.6	28.4	69
Kamb	C	16.7	0	50.6	14.1	84
	TC1	40.1	0	64.5	26.4	66
	TC2	89.7	0	51.5	84.4	94
Bindschadler	D	10.0	0[b]	125.1	6.0	60
	TD1	67.8	16	94.1	52.5	77
	TD2	29.0	37	105.5	20.5	71
	TD3	31.0	0	67.4	23.8	77
MacAyeal	E	15.3	26	126.1	12.3	81
	TE	44.9	23	113.7	30.9	69

[a] Inferred by *Joughin et al.* [2002], $\tau_{grav} = \rho_{ice}gHS$ where S is the downstream slope.

[b] The ratio increases to $\sim 53\%$ when evaluated 30 km downstream (see text).
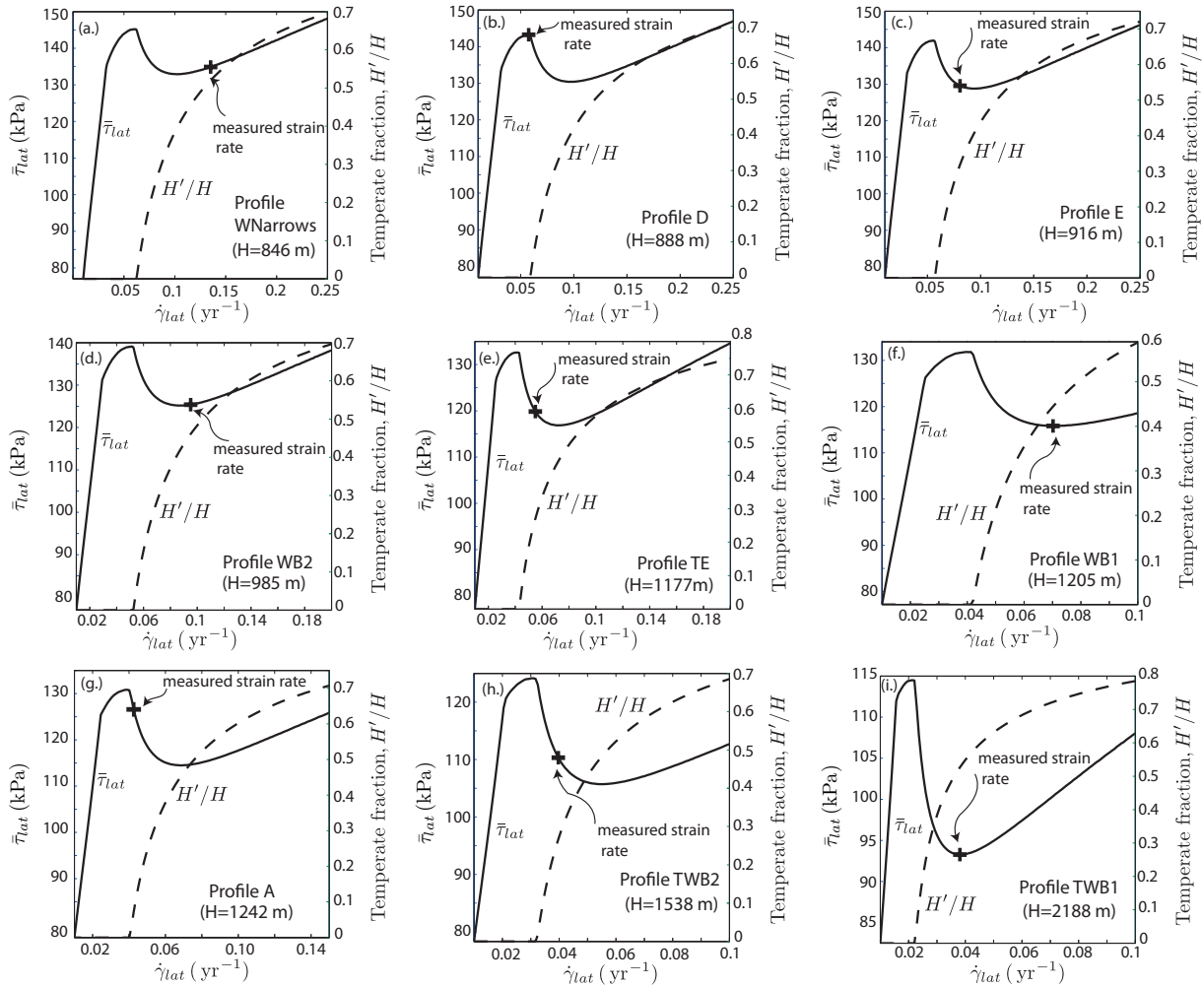
Figure 7. Triple valued lateral shear stress (solid line) and temperate fraction of the ice sheet thickness (dashed line) versus shear strain rate. The strain rate is used as an input to find the temperature profile, which gives H' and hence the lateral shear stress averaged over the ice thickness. Simulations are performed for all the profiles listed in Table 1 using their corresponding thicknesses (ordered by increasing H here). Maxima in solid line curves correspond to the onset of a temperate zone. We also indicate the shear strain rate at the margins of the profiles measured by *Joughin et al.* [2002] (black cross).

Profile E of MacAyeal ice stream shows that this stream is wider than the other active ice streams (with the exception of the ice plain of Whillans IS), which seems to diminish the influence of lateral drag ($\bar{\tau}_{base}/\tau_{grav} = 81\%$). The effect of temperate ice over 203 m at the margin increases only by 1.5 kPa the predicted basal drag assuming frozen margins [*Joughin et al.*, 2002]. However, at MacAyeal ice stream much of the resistance is concentrated at a few sticky spots where $\bar{\tau}_{base}$ reaches 50 kPa [*Fricker et al.*, 2010]. Nevertheless, our estimation of the average basal shear stress over the width of 15.3 kPa is in accordance with control method inversions for a plastic bed over this region (14.9 kPa according to *Joughin et al.* [2003]).

These basal shear stresses are calculated as an average over the width. Small scale perturbations of $\bar{\tau}_{base}$ occur as a result of the water pore pressure in the till, assuming that subglacial drainage is partly made of distributed flow and channelized drainage [*Schoof*, 2010; *Hewitt*, 2011]. Also, the numbers reported for $\bar{\tau}_{base}$ should be thought of as a combination of the actual $\bar{\tau}_{base}$ plus a poorly constrained contribution to overall force equilibrium from gradients in net axial force.

Finally, a remarkable result arises from equation (14). That result argues that the basal shear stress must be non-uniform, and enhanced as the margin is approached from within the fast-moving stream. When plotting the average lateral shear stress based on our thermal modeling versus a large range of shear strain rate for a given H, numerical simulations suggest a triple-valued law (Figure 7) relating $\bar{\tau}_{lat}$ to $\dot{\gamma}_{lat}$. The shear stress increases with increasing strain rate before onset of melting. Once the work associated with lateral deformation of ice is sufficient to melt the ice at the base ($H'/H > 0$), $\bar{\tau}_{lat}$ decreases due to thermal softening. For larger strain rates, strain rate hardening becomes dominant and $\bar{\tau}_{lat}$ again increases with $\dot{\gamma}_{lat}$. We find that such a triple-valued law appears for ice sheet thicknesses larger than 300 m for an accumulation rate of 0.1 m.yr^{-1} and 200 m for $a = 0.2$ m.yr^{-1}. Since SCIS thicknesses are higher than 800 m, it is most likely that such triple-valued law exists. We perform simulations using the thicknesses of SCIS listed in Table 1 and display nine of the sixteen profiles such that the thicknesses used for the simulations span the entire range of H. We observe that most of the margins of SCIS experience a level of straining at which we predict the side drag to sit in the region of locally reduced shear stress due to thermal softening. These results are intriguing. A conjecture, meriting further examination, is that this local minimum may be related to the location of a drainage channel at the bed that would strengthen the bed (see next subsection 3.4.2 for details) to support the locally reduced side drag. This triple-valuedness of $\bar{\tau}_{lat}$ as a function of $\dot{\gamma}_{lat}$ is unrelated to recent hypotheses of triple-valued relation between τ_{base} and the downstream basal velocity u_b [*Sayag and Tziperman*, 2009; *Kyrke-Smith et al.*, 2014]. Our modeling here has a negligible dependence of τ_{base} on u_b, regarding it as mainly a function of basal effective stress, which we argue, as follows, to vary substantially at a partially melted margin.

# 3. Could melt onset control ice stream width?

Continuous deformation of temperate ice at the margins generates meltwater, which gravity would cause to percolate toward the bed below. In this section, we estimate the accumulated seepage rate along the bed of Dragon margin, the southern margin of Whillans IS B2. For this, we use a transverse profile of shear strain rate [*Echelmeyer et al.*, 1994] across the margin as an input for our simple 1-D thermal modeling. This produces a 2-D temperature field of the Dragon margin (subsection 3.1). Equating the stress working with latent heat in the temperate region, we quantify

the meltwater production. Associated with seeping water along the margin's bed, a channelized marginal drainage of Röthlisberger type may develop, plausibly under the chaotic crevassing zone where the shear heating, and corresponding basal meltrate, is the highest [*Beem et al.*, 2010] (subsection 3.2). Standard theory argues that the high, nearly litho-static, pore pressure elsewhere (i.e., near the bed within the fast moving stream), is somewhat alleviated within the channel, which operates at reduced water pressure [*Röthlisberger*, 1972; *Nye*, 1976]. This results in a higher Terzaghi effective normal stress acting along the bed just outside of the channel, hence, creating high resistance against frictional shear, which plausibly locks the ice inboard and outboard of such a channel to the bed, naturally forming an ice stream margin (subsection 3.3). We suggest that if other SCIS experience such high strain rates localized at their margins, we could generalize this mechanism to all SICS. We suggest that such channelized drainage, and the related zone of reduced pore pressure (hence, of larger effective stress and shear strength) adjoining it, may more firmly lock the ice to the now stronger bed. Such increased bed resistance near the margin, required if the margin has to carry less $\bar{\tau}_{lat}$ than the adjoining ice within the fast-flowing stream (as in Figure 7), may be a factor in slowing lateral migration of the margin (subsection 3.4).

3.1. Detailed characterization of Dragon margin, Whillans IS B2

Dragon margin, an approximately 4 km wide marginal shear zone, is the southern margin of Whillans IS B2, the limit between the stream and the ridge B1-B2 named Unicorn (Figure 6). The inner-boundary of this margin is approximately a 2 km wide region of large, but somewhat organized, crevasses whose density increases toward the margin. These crevasses roughly tend upstream at an angle of 40 ° to 70 ° to the margin. This sub-zone ends rather abruptly at the chaotic zone. This last zone of approximately 2 km width consists of highly disorganized crevasses and fractured ice blocks, a signature of elevated lateral shear stress. The outer boundary of Dragon margin, a sub-zone of $\sim$ 100 m width [*Echelmeyer et al.*, 1994], consists of large but widely spaced crevasses. We do not represent this narrow sub-zone on Figure 6 or Figure 8. Profile S1, near to, but not the same as the WB2 profile, gives us a transverse profile of the downstream velocity. Over a 5 km distance, the velocity decreases from 387 m.yr^{-1} at the northern extremity of profile S1 to 2 m.yr^{-1} just outside of the margin (i.e., south S1). In this domain, the lateral shear strain rate varies from 0.01 to 0.15 yr^{-1} (Figure 8a). Between the middle of the stream and north of S1, the surface velocity observed does not change significantly (i.e., the lateral strain rate is close to zero). This profile gives us an excellent set of data to characterize the behavior of a margin, we will use it in the rest of the paper.

We use our 1-D model to produce a profile of temperature versus height and show the fraction of the ice sheet near the margin, which we predict to be temperate. The calculations are, of course, approximate because the 1-D model is most accurate at long (compared sheet thickness) spatial wavelengths in the lateral direction. We find that temperate ice at Dragon margin is predicted to reach a maximum 57% of the ice sheet thickness and to be comparably high over slightly more than 2 km width at the bed (Figure 8a). In this simplified thermal modeling, the width of temperate ice through the ice sheet approximately matches the width of the highly stressed chaotic crevassing zone that appears at the surface.
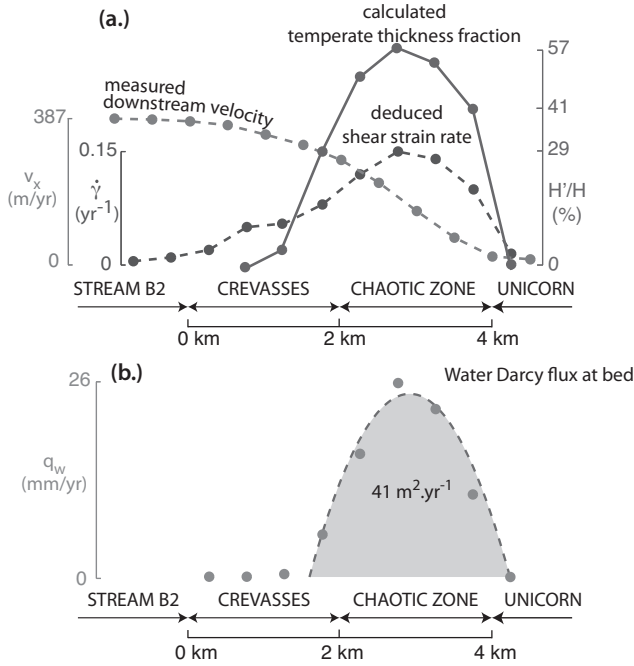
Figure 8. Detailed characterization of Dragon margin (profile S1 located on Figure 6). (a.) Measured downstream velocity gives the lateral shear strain rate profile [*Echelmeyer et al.*, 1994]. Then, this is inserted into our simple 1-D thermal model of a partially melted margin, which considers a constant ice sheet thickness $H = 985$ m, to estimate the temperate fraction H'/H and melting profile. Where the lateral strain rate is the highest (0.15 yr^{-1}) in the chaotic crevassing zone, 57% of the ice sheet thickness is temperate. Vertical motion (advection) of ice may thus occur, with assumed accumulation in order to keep the thickness at steady state, and our approximate advection profile may be still valid there. (b.) Darcy water flux at base of temperate ice calculated with equation (20) (circles). We predict that the shear heating could melt the near-bed ice over a 2 km width under the chaotic crevassing zone, producing a water flux, integrated across the base of the margin, of about 41 m^2.yr^{-1} (second-order polynomial fit).

This simplified 1-D thermal modeling assumes a constant strain rate with depth, neglects horizontal diffusion and advection and possible margin migration [*Echelmeyer and Harrison*, 1999; *Harrison et al.*, 1998]. Whilst the authors are aware of the roughness of the estimations provided for the size of the deformation-induced temperate zone at Dragon margin, we compare in Figure 9 our predictions with our more elaborate, but distinct, 2-D thermal modeling of the same margin reported in *Suckale et al.* [2014]. In the mentioned paper, the thermal regime of Dragon margin is calculated using a 2-D thermomechanical model of an ice stream flowing over a plastic bed at steady state. This model accounts for multiple deformation mechanisms depending on the level of stresses and for temperature-dependent ice properties. The heat analysis includes the horizontal diffusion neglected in the present study. *Suckale et al.* [2014] assume a uniform basal resistance for which the magnitude is adjusted to give the most plausible fit to the velocity profile measured at the surface (Profile S1), and predict in this case the temperate zone displayed in Figure 9 that matches reasonably well the one we calculate in this study. However, because the 1-D model seems to overestimate the size of the

temperate region, we discuss, later in the text, the sensitivity of the locking process to the amount of water generated (directly related to the size of the temperate zone). Also, we conclude from the triple-valued relation of $\bar{\tau}_{lat}$ to $\dot{\gamma}_{lat}$ and consideration of force equilibrium, that the basal shear stress must have an important deviation from uniformity as the margin is approached.

3.2. Drainage to the bed associated with melting causes Röthlisberger channel development

Within the temperate ice column of height H', water permeation occurs. Shear heating generates melt at a rate per unit of volume $\dot{m}$. Thus,

$$\dot{m} = \frac{\tau_{lat}\dot{\gamma}_{lat}}{L_f} \tag{16}$$

where $L_f = 335$ kJ.kg^{-1} is the latent heat per unit mass. Water in polycrystalline ice at its melting point forms a system of veins at three-grain junctions [*Nye*, 1989]. This water, both in veins and in other locations, may affect the creep rate of temperate ice, although we ignore this for now. Then the creep strength in temperate ice within the height H' is

$$\tau_{lat} = A_{melt}^{-1/3} \left(\frac{\dot{\gamma}_{lat}}{2}\right)^{1/3}, \tag{17}$$

and the melt rate per unit of volume becomes

$$\dot{m} = \frac{2A_{melt}^{-1/3}}{L_f} \left(\frac{\dot{\gamma}_{lat}}{2}\right)^{4/3}, \tag{18}$$

where $A_{melt}^{-1/3}$ is 244 kPa.yr$^{1/3}$ for a melting temperature of $-0.6°$C at Dragon margin's bed. Meltwater, being more dense than its chemically identical solid phase (neglecting any contamination from above), seeps downward. Considering only the vertical Darcy flux q_w of water, mass conservation $\nabla \cdot (\rho_w q_w) = -\dot{m}$ leads to

$$\frac{dq_w}{dz} = -\frac{2A_{melt}^{-1/3}}{\rho_w L_f} \left(\frac{\dot{\gamma}_{lat}}{2}\right)^{4/3} \tag{19}$$

with $\rho_w = 1000$ kg.m^{-3} the density of water. This latter equation is integrated in z over the temperate ice thickness to find the downward Darcy flux at the bed q_{temp}, assuming again that the shear strain rate is uniform over depth and knowing that the Darcy flux vanishes at the top of the temperate ice column. Thus,

$$q_{temp} = \frac{2\,A_{melt}^{-1/3}\,H'}{\rho_w L_f} \left(\frac{\dot{\gamma}_{lat}}{2}\right)^{4/3}. \tag{20}$$

The Darcy water flux at the base of an ice column where internal melting occurs is only a function of the shear strain rate, and the height of temperate ice, which we predicted with our previous thermal modeling allowing for a temperate zone. Using the transverse profile of observed strain rate and calculated temperate height H' of ice adjoining the bed, at the Dragon margin depicted graphically in Figure 8a, the last equation gives a transverse profile of the basal meltwater rate (cf. Figure 8b). This deformation-induced seeping meltwater is localized only under the highly stressed chaotic crevassing zone where the maximum Darcy flux reaches 26 mm.yr^{-1}. That is an order of magnitude higher than the estimated basal meltwater rate due to basal friction inferred to be present at the center of this stream [*Joughin et al.*, 2003] and other SCIS [*Joughin et al.*, 2004b]. Nevertheless, the melt production due to basal friction acts over a great
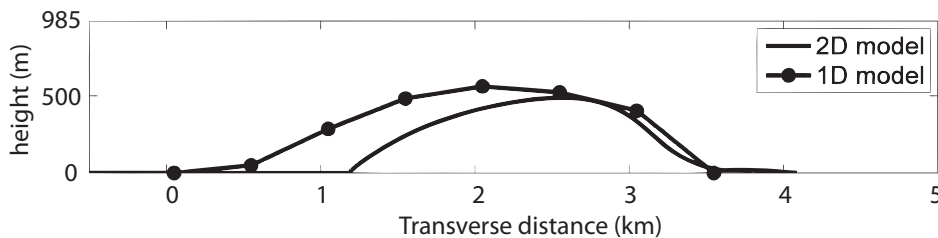
Figure 9. Comparison of the size of the temperate zone at Dragon margin (Profile S1), plotted on a 1:1 scale, between our simplified 1-D thermal modeling that assumes a constant strain rate with depth and the more elaborate 2-D thermal modeling by *Suckale et al.* [2014] (see details in text). Both simulations are done with an accumulation rate of 0.1 m/yr.

width and should feed a hydrologic system which, while principally flowing downslope, will also have a transverse component of flow towards any zone of locally reduced pore pressure associated with channelized drainage at the margin (subsection 3.4).

Vogel et al. [2005] drilled to the bottom of Kamb IS at the transition between the active upper part and its stopped main trunk (cf. Figure 2), and found that basal ice is devoid of air. We suppose that, at the base of the ice sheet, the veins are water saturated and the ice grains slide at their boundary allowing the water pressure to be equal to the ice overburden stress. This sliding allows the permeability to adjust to whatever value is needed to transmit the meltwater generated, at least for a system operating in steady state. Along the bed, the total downward flux of meltwater per unit area produced by shear heating may be expressed as in Darcy's law,

$$q_w = -\frac{k_{ice}}{\mu_w}\left(\frac{dp}{dz} + \rho_w g\right) \qquad (21)$$

where $\mu_w = 1.8 \times 10^{-3}$ N.s.m^{-2} is the dynamic viscosity of water and g the acceleration due to gravity. Assuming the water pressure in veins is equal to the ice overburden pressure, $dp/dz = -\rho_{ice}g$. Thus, the required temperate ice permeability, a function of the downward water Darcy flux, is

$$k_{ice} = \frac{q_w\,\mu_w}{(\rho_{ice} - \rho_w)\,g}. \qquad (22)$$

The Darcy flux estimated at the Dragon margin bed is about 26 mm.yr^{-1} (Figure 8b). Therefore, we find a maximum ice permeability of 1.7×10^{-15} m^2, consistent with measurements of water saturated veins (*Jordan and Stark* [2001] found temperate ice permeability of 1 to 3×10^{-15} m^2).

According to *Nye and Frank* [1973], for a given k, the porosity is proportional to d_g^{-1}, where d_g is the grain size. Our estimation of the permeability at the bed of the ice sheet at the margin is compatible with a porosity of 1.6×10^{-3} for a grain size of 1 cm and 1.6×10^{-5} for a grain size of 1 mm. These values, certainly for $d_g = 1$ mm, and likely for $d_g = 10$ mm, seem small enough that we can assume that the porosity we encounter has a negligible effect on the ice rheology.

We integrate the meltwater generated along the bed by shear heating over the width of the highly stressed temperate zone of the Dragon margin where sampled (Figure 6). We find that 41 m^3.yr^{-1} of meltwater emerges, along the ice-till interface, for each meter of length downstream (cf. Figure 8b).

We suggest that the relatively high, localized, water production found at the bed could cause a channelized marginal drainage development of Röthlisberger type (R-channel), which would collect the 41 m^2.yr^{-1} of meltwater produced over each meter of length downstream. For a simple model

of the process, we assume that the water pressure gradient in the channel is negligible (flow is driven only by the downslope component of gravity), and we quantify what would be the diameter of such subglacial conduit after collecting a comparable meltrate over several kilometers upstream. Using the Manning formula for a turbulent rough-walled channel flow, neglecting any water pressure gradient, and letting Q_w (m^3.yr^{-1}) be the water discharge rate, the mean flow velocity is

$$\frac{Q_w}{A_c} = \frac{R_h^{2/3}S^{1/2}}{n_m}, \qquad (23)$$

where R_h is the hydraulic radius, A_c refers to the cross-sectional area, n_m, in s.m$^{-1/3}$, is the Gaukler-Manning-Strickler roughness coefficient and S the absolute value of the downstream slope. In this present work, the channel is assumed to be melted into the ice and semicircular; hence, as pointed out by *Clarke* [2003], the Manning roughness coefficient is a wetted-perimeter-average value allowing distinction between the roughness of the ice wall, of wetted perimeter $\pi D/2$, and the bed wall of perimeter D. Also, R_h, the hydraulic radius (ratio of A_c to wetted perimeter) is, for the considered semicircular channel of diameter D,

$$R_h = \frac{D}{4(1 + 2/\pi)}. \qquad (24)$$

Thus, the diameter of this semicircular channel of constant water pressure that drains a flux Q_w is

$$D = \frac{2^{13/8}\,(Q_w\,n_m)^{3/8}\,(1 + 2/\pi)^{1/4}}{\pi^{3/8}\,S^{3/16}}. \qquad (25)$$

If this tunnel collects from 100 km upstream a constant supply of 41 m^3 per meter downstream per year (as in Figure 8b), the volumetric discharge rate would be $Q_w = 41$ m^2.yr$^{-1}\times$ 100 km=0.13 m^3.s^{-1}. We adopt the slope S of Whillans IS B2 measured near Up B (Figure 6) of 0.00123 [*Joughin et al.*, 2002]. Thus, the last parameter that needs to be constrained is the Manning roughness coefficient. Because this seems to be often overestimated in subglacial conduits [*Clarke*, 2003], we divert here to a brief discussion about plausible values for our considered subglacial drainage system.

Assuming a rough turbulence, that is, a high Reynolds number range in which $(2\tau_{wall})/(\rho_w U^2)$ is independent of viscosity (U is the average fluid velocity) and, hence, independent of further changes in Reynolds number, we recall the Darcy-Weisbach friction factor f_{dw},

$$\tau_{wall} = \frac{1}{8}f_{dw}\rho_w U^2, \qquad (26)$$

where τ_{wall} is the wall stress acting over the wetted perimeter,

$$\tau_{wall} = \rho_w gSR_h. \qquad (27)$$

Table 3. Semicircular channel diameter D, and Terzaghi effective stresses N_c in till at its borders, for different discharge rates Q_w and Manning coefficients n_m (with corresponding Nikuradse roughness amplitudes k shown). Till shear strength $\tau_{ch} \approx 0.5\, N_c$ at channel borders, which is 12 to 56 times higher than the basal shear stress inferred under the ice stream center.

Parameter	notation (units)	values			
Manning coefficient	n_m (s.m$^{-1/3}$)	0.01	0.02	0.03	0.04
Equivalent Nikuradse roughness	k (cm)	0.03	1.6	18.0	101.1
Water discharge of $Q_w = 0.13$ m^3.s^{-1}					
Channel diameter	D (m)	0.9	1.1	1.3	1.5
Terzaghi effective stress	N_c (kPa)	369	310	280	261
Water discharge of $Q_w = 0.03$ m^3.s^{-1}					
Channel diameter	D (m)	0.5	0.7	0.8	0.9
Terzaghi effective stress	N_c (kPa)	326	274	248	231

Furthermore, fitting the Gaukler-Manning-Strickler expression to the Nikuradse experiments on rough-walled turbulent pipe flow ($Re > 10^5$) (see, e.g., *Gioia and Chakraborty* [2006]), for ratio of R/k from 15.0 to 507 (R being the pipe radius and k the Nikuradse wall-roughness amplitude with unit of length), that is for f_{dw} ranging from 0.06 to 0.02, shows

$$n_m \approx \frac{k^{1/6}}{8g^{1/2}}. \qquad (28)$$

Hence, the Manning roughness coefficient range inferred by *Clarke* [2003] for subglacial flooding of 0.02 to 0.04 s.m$^{-1/3}$ corresponds to equivalent Nikuradse roughness of 1.6 to 101.1 cm (see Table 3). A wall roughness of 101.1 cm caused by large blocks of ice is rather sensible for a subglacial flooding event; however, in our subglacial drainage case, we assume a plausible range of 0.02 to 0.03 s.m$^{-1/3}$ for n_m corresponding to a Nikuradse roughnesses of 1.6 to 18.0 cm.

The accumulated seepage along the bed at the estimated rate at Dragon margin sampled by *Echelmeyer and Harrison* [1999] (41 m^3.yr^{-1} for each meter of length downstream), if prevailing over 100 km upstream, is consistent with a semicircular Röthlisberger channel of diameter $D = 1.1$ m (for $n_m = 0.02$ s.m$^{-1/3}$) to $D = 1.3$ m (for $n_m = 0.03$ s.m$^{-1/3}$) (see Table 3). A sensitivity analysis on chosen parameters and effects on results is developed in subsection 3.3.

3.3. Limit to the stream width by strengthened ice-bed interface adjacent to marginal channels

As predicted by the standard theory of a subglacial drainage system, a greater melt supply to a channel results in a higher discharge and, thus, a lower water pressure in and nearby the conduit. If a R-channel at the ice stream's margin collects a relatively high amount of meltwater generated by shear heating, this would induce a high Terzaghi effective stress along the ice-till interface just outboard of the channel. We intend here to evaluate this Terzaghi effective stress adjacent to a hypothetical semicircular channel at the margin's bed, for a given volumetric water discharge rate Q_w, using simplified equations from steady-state tunnel theory [*Röthlisberger*, 1972; *Nye*, 1976].

Again, we assume that the rough turbulent flow in the channel of slope S is gravity driven and the water pressure p_{ch} is approximatively independent of the distance downslope. We also consider the water temperature is equal to the ice wall temperature (i.e., at the melting point). The energy dissipation at a rate of $\rho_w gSQ_w$ in flow supplies latent heat L_f to melt the ice wall of the semicircular pipe; hence, the channel radius $D/2$ increases at a rate u_{melt} where,

$$L_f \rho_{ice}(\pi D/2)\, u_{melt} = \rho_w gSQ_w. \qquad (29)$$

In addition, the channel radius decreases by creep closure [*Nye*, 1953] at a rate u_{creep} such as,

$$u_{creep} = \frac{D/2}{27} A_{melt} \left(\sigma_0 - p_{ch}\right)^3, \qquad (30)$$

recalling that A_{melt} is the creep parameter at the melting point and σ_0 is the ice overburden pressure . At steady state, the inflow of ice is balanced by the melting of the ice wall, $u_{creep} = u_{melt}$; hence, we have,

$$\left(\sigma_0 - p_{ch}\right)^3 = 27\, \frac{\rho_w gSQ_w}{\pi L_f\, \rho_{ice}\, A_{melt}\, (D/2)^2}. \qquad (31)$$

The hoop stress σ_{hoop} at the channel's wall cut into the ice satisfies $\left(\sigma_{hoop} - p_{ch}\right) = (2/3)(\sigma_0 - p_{ch})$ [*Nye*, 1976]. Since Q_w and the channel diameter are related by the Gaukler-Manning-Strickler formulae, see equation (25), we finally find the Terzaghi effective stress $N_c = (\sigma_{hoop} - p_{ch})$ just outboard of the channel,

$$N_c = \frac{2}{3} K_2\, \frac{Q_w^{1/12}\, S^{11/24}}{n_m^{1/4}\, A_{melt}^{1/3}} \qquad (32)$$

with,

$$K_2 = \left(\frac{\rho_w g}{\rho_{ice} L_f K_1}\right)^{1/3} \qquad (33)$$

and $K_1 = (2/27)\, (2\pi)^{1/4}\, (1 + 2/\pi)^{1/2}$.

We again consider a semicircular channel cut into the ice that collects from 100 km upstream a constant water supply as generated at Dragon margin near Up B (i.e., 0.13 m^3 .s^{-1} per meter length downstream). Downstream, this meltrate is consistent with a Terzaghi effective stress just outboard of the subglacial conduit going from 280 to 310 kPa with reasonable Manning coefficients (see Table 3). Moreover, the width-averaged basal drag we inferred at the Whillans B2 center is 3.7 kPa (cf. Table 2); hence, a rough approximation of the basal effective stress at Whillans B2 centerpart becomes $((\bar{\tau}_{base} - c)/f) = 5.4$ kPa assuming a till friction coefficient of $f = 0.5$ [*Rathbun et al.*, 2008] and a till cohesion of $c = 1$ kPa [*Kamb*, 2001]. Therefore, the effective stress near the considered channel of diameter $D = 1.1$ m is 57 times larger than the predicted effective stress at the center of the Whillans IS B2. This high effective stress outboard of such a marginal R-channel creates high resistance against frictional basal shear, firmly pressing the ice against the till bed.

We note from equations (25) and (32) the dependence of the diameter D of the hypothesized channel, and the Terzaghi effective stress N_c just outboard of it, on the water discharge rate Q_w and Manning factor n_m. As shown in the more elaborate 2-D thermomechanical model of Dragon

margin by *Suckale et al.* [2014], the size of temperate region and, hence, the meltwater generated at the bed varies significantly with factors such as margin migration or surface crevassing (see subsection 4.2). Also, some marginal melt may migrate toward the center of the ice stream due to the transverse slope of the bed and ice surface near the margin [*Le Brocq et al.*, 2009; *Fricker and Scambos*, 2009]. Although such flow tendency is resisted by the greatly reduced pressure in the channel, making it a line sink for the subglacial water seepage (cf. subsection 3.4.2). Considering the uncertainties, we may overestimate the meltwater production at the bed. However, we find that reducing the estimated value of Q_w by a factor 4 results in only a 11% reduction of N_c and a 41% reduction in D (Table 3). In this case, we calculate a shear strength next to the channel at the bed of Dragon margin 50 times higher than the strength under the corresponding ice stream for a reasonable Manning coefficient of 0.02 s.m$^{-1/3}$ and $f = 0.5$ [*Rathbun et al.*, 2008] (and 46 times if $n_m = 0.03$ s.m$^{-1/3}$). Therefore, our estimates of bed strength next to the channel and D are not strongly sensitive to the assumed magnitude of the channelized water flux Q_w.

3.4. Stabilizing mechanisms at the margin: a crack problem

3.4.1. Marginal channel and crack tip blunting

Ice streams are underlain everywhere by a plastic bed [*Tulaczyk et al.*, 2000]. If the basal shear stress equals the yield strength of the bed everywhere under the stream, then downslope sliding occurs while the ridges are locked, frozen to the bed. This anti-plane shear crack-like feature (see Figure 10) induces stress singularities at the margins. High stress concentrations on the ice-stream side of the margin have been found either analytically when considering the ice as a Newtonian fluid with constant viscosity [*Schoof*, 2004, 2012] and numerically when ice rheology is treated
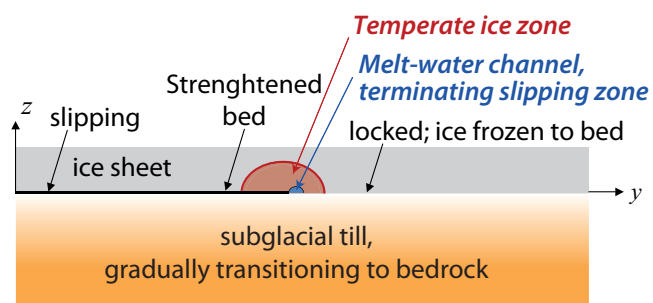
Figure 10. Conjectured stable configuration (not to scale) of an ice stream shear margin near the bed. The transition between slipping and locked zones at an ice sheet bed defines an anti-plane shear crack whose surface is the base of the ice sheet beneath the streaming flow (thick black line) and whose tip lies along the shear margin. Because cracks strongly concentrate stress and strain rate near their tips, the shear heating and, hence, the basal meltwater generation should be most intense in that near-tip region and may induce meltwater channel formation. Both standard theory of fracture mechanics and hydrology argue that this channel development would contribute to resistance to any continued expansion of the slipping zone. A crack ending in a channel has a greatly diminished stress and strain rate concentration, compared to a sharp-tipped one, and the high Terzaghi effective stress just outside the channel operating at low pressure increases the shear strength of the till bed.

with Glen's law [*Jacobson and Raymond*, 1998; *Suckale et al.*, 2014]. To prevent the shearing crack growth due to high stress concentration at the tip, we note that standard theory of fracture mechanics argues that a large enough hole in a thin plate can stop a tensile crack that is growing in the plate. The crack can grow into a hole but not propagate out easily because then the stress concentration at its tip is much reduced. We may think of the ice stream and bed as an analogous system, now containing an anti-plane crack whose surface is the base of the ice sheet beneath the stream and whose tip lies along the shear margin. We suggest that one way to stop an outward propagation of such a crack, that is, to stop outward margin migration, is to alleviate the stress concentration at the crack tip. That would be accomplished by having the tip region be replaced by a long marginal channelized drainage such as we have suggested, leaving a situation analogous to a crack whose tip has propagated into a hole (cf. Figure 10).

Our preliminary studies [*Perol et al.*, 2012] suggest that realistic channel hole sizes, while greatly reducing stress, could not of themselves prevent basal slip from spreading outward beyond the channel treating the ice as a Newtonian fluid. Also, *Perol et al.* [2012] show that having a semicircular channel would be the more efficient in reducing the basal shear stress acting on its border than other shapes, e.g., elliptical channel and basal crevasses.

3.4.2. Marginal channel and Dugdale-Barenblatt cohesive zone model

Another important factor, contributing to stabilizing the configuration against slip propagation beyond the (hypothesized) channel is the elevated Terzaghi clamping stress that we have estimated along the bed. The channel at the tip of the anti-plane crack operating at low pressure captures some of the water generated at the ice-till interface by frictional sliding, the rest being evacuated downstream. The induced pore pressure profile at the ice-till interface creates a situation in which the till strength matches the low basal shear stress inverted previously under the ice stream far away from such channel (in the case of Dragon margin, $\bar{\tau}_{base}$ of profile WB2 reported in Table 2) and the high strength $fN_c + c$ due to low water pressure just outboard of it. This crack resistance feature, similar to the Dugdale-Barenblatt cohesive zone concept in fracture mechanics [*Barenblatt*, 1959; *Dugdale*, 1960; *Bilby et al.*, 1963], contributes to alleviate the stress concentration (a stress singularity for the mathematical model of a planar crack with a sharp tip) created by the freely slipping to locked bed transition. In this subsection we build a simplified subglacial hydrological model at the ice-till interface surrounding the channel and under the stream to quantify such till strength profile. Then we ask whether this crack resistance is sufficient to remove the stress singularity at the margin, pinning the margin at its current location. Again, we note that such enhanced basal resistance near the margin is required by the triple-valued $\bar{\tau}_{lat}$ vs $\dot{\gamma}_{lat}$ relation, particularly when the inferred $\bar{\tau}_{lat}$ at the margin is in the low-strength valley in the curve in Figure 7.

We again consider a cross section of an ice stream slab of constant surface slope flowing over a layer of till (like in Figure 1) that behaves as a Coulomb-Plastic material. We assume that the till transmissivity would not be sufficient enough to alleviate the important amount of water generated by frictional sliding and englacial meltwater seepage from temperate ice. Therefore we suppose that a thin water layer of thickness h of mm scale exits at the interface inbetween ice and till [*Weertman*, 1972; *Le Brocq et al.*, 2009]. One can note that this theoretical prediction first introduced by *Weertman* [1972] may find support from observations at the bed of Kamb ice stream where *Vogel* [2004] observed that the over-pressure in the borehole was enough to lift the ice from the bed by a mm to cm scale suggesting a very strong

dependence of the hydraulic transmissivity of the till to the normal effective stress when this latter one is near zero. The rough-bedded film adopted here and studied by *Creyts and Schoof* [2009] and *Kyrke-Smith et al.* [2014] supports the ice flow through large clasts that are probably few cm apart and hence, the ice-till contact is done via these till clasts. We define $\hat{y}$ transverse to the flow starting at the channel and negative under the ice stream ($\hat{y} = y - W/2$). The hat highlights the distinction with the coordinates system used for thermal modeling. Based on the hydrological model developed in Appendix B the form of this till strength profile under the stream satisfies

$$G_{geo} - (T_{melt} - T_{atm}) \left(\frac{\rho_{ice} C_i K}{\pi t_0} \right)^{1/2} + \tau_{base} u_b \qquad (34)$$

$$+ \rho_w L q_{temp} = \frac{T_{wf} L_f}{f g} \frac{\partial^2 \tau_{base}}{\partial \hat{y}^2}$$

G_{geo} is the geothermal heat flux, typically $G_{geo} = 70$ mW.m^{-2} [*Engelhardt*, 2004; *Maule et al.*, 2005] in the Siple Coast region. The thermal conductivity K and the heat capacity C_i are taken at their melting point value. c is the cohesion estimated at 1 kPa by *Kamb* [2001], q_{temp} is the melting rate profile due to temperate ice above, depicted in Figure 8. $T_{wf} = (h^3 \rho_w g)/(12\mu_w)$ (see Appendix B) is the transmissivity of the water film. The second term in equation (34) represents heat flow into the thermal boundary layer at the glacial bed, which has developed over the lifetime t_0 of the stream and, for realistic choices of t_0, is still small compared to the ice sheet thickness $H \approx 1$ km. u_b is the basal velocity profile.

The basal velocity profile is taken to be the one measured by *Echelmeyer et al.* [1994] at the surface and partially reproduced in Figure 8. The velocity vanishes at the channel, marker of the transition between slipping to locked bed and increases following the surface velocity curve. This is of course an approximation. One would have to solve the anti-plane shear flow with the appropriate fluid rheology to find the velocity at the base of the ice sheet. Sufficiently away from the channel the strain rate becomes uniform over depth, hence, there, taking the surface velocity is a reasonable first approximation. However, close to the channel located at the crack tip analog, basic results from fracture mechanics show that the velocity profile is steeper than at the surface.

As explained in Appendix B, t_0 is the time scale for the development of conductive heat lost through the ice sheet at its base due to the temperature gradient between the surface and the bottom. We calculate t_0 such that the asymptotic limit of the basal shear τ_{base} in equation (34) reaches the value prescribed under the stream. Far away from the channel, $\tau_{base} = \bar{\tau}_{base} = 3.7$ kPa (see Profile WB2 in Table 2) and the basal velocity reaches its maximum value $u_{max} = 428$ m/yr, the dominant balance of equation (34) is

$$G_{geo} - (T_{melt} - T_{atm}) \left(\frac{\rho_{ice} C_i K}{\pi t_0} \right)^{1/2} + \bar{\tau}_{base} u_{max} = 0 \quad (35)$$

which gives $t_0 = 1439$ yr. Equation (34) is solved numerically with $\tau_{base}(\hat{y} = 0) = f N_c + c$ and by shooting for the derivative that matches the asymptotic solution $\tau_{base} = \bar{\tau}_{base} = 3.7$ kPa.

Assuming a high Terzaghi clamping stress of 300 kPa next to the channel in agreement with previous estimations, the strength profiles are plotted in Figure 11. Profiles for $h \leq 0.4$ mm are not physical as they predict water pressures above the ice overburden pressure that would lift the ice next to the channel. Recalling that the half-width of Whillans IS B2 is 17 km and enforcing the water pressure to not exceed the overburden pressure, our results constrain the water thickness to be between 0.4 and 1 mm. These profiles predict till strengths greater than the driving gravitational stress

over 1 to 4 km distance (respectively for $h = 0.4$ mm and $h = 1$ mm) to the crack tip analog, which could possibly remove the stress singularity according to *Schoof* [2004], by the same process as in the Dugdale-Barenblatt model.

Such increased bed resistance near the margin is, in fact, required if the margin has to carry less lateral shear stress than the adjoining ice within the fast-flowing stream. The triple-valued law plotted in Figure 7d shows that, when entering the shear margin, the level of straining is high enough to thermally weaken the margin. The reduction of lateral drag would act over a width δ scaling with the margin width. Our simulations show that the lateral shear stress averaged over the thickness decreases when entering the shear margin by about $\Delta \bar{\tau}_{lat} = 15$ kPa. A simple force balance predicts that an enhanced basal shear is therefore needed to support the gravitational force. Considering a block of ice of thickness H and width $\delta = 1$ km at the margin on which the variation in lateral stresses is $\Delta \bar{\tau}_{lat}$, we evaluate a enhanced basal shear stress of $\Delta \tau_{base} = \tau_{grav} + (H/\delta) \Delta \bar{\tau}_{lat} \approx 25$ kPa. This enhanced bed strengthening due to margin weakening is coherent with a profile calculated for a water thickness $h = 0.4$ mm.

We use a path-independent integral J_{tip} to calculate the magnitude of the stress singularity at the crack tip analog. This J-type integral, first introduced in the context of crack in (possibly non-linear) elastic materials [*Rice*, 1968a, b; *Cherepanov*, 1968; *Bilby and Eshelby*, 1968], has been generalized in the context of non linear creeping solids [*Goldman and Hutchinson*, 1975; *Landes and Begley*, 1976; *Kubo et al.*, 1979; *Ben Amar and Rice*, 2002] and ice flow [*McMeeking and Johnson*, 1986]. It is relevant in our anti-plane shear flow of ice linking the far-field loading on the ice stream to the stress singularity near the transition from a slipping to a locking bed. *Suckale et al.* [2014] show in Appendix C equation (C3) that

$$\frac{J_{tip}}{2} = \tau_{grav} u_{max} + \int_{-W/2}^{0} \tau_{base}(\hat{y}) \frac{\partial u_b}{\partial \hat{y}} d\hat{y}. \qquad (36)$$

where $u_b(\hat{y} = -W/2) = u_{max} = 428$ m/yr. The second term in the right-hand side is a negative contribution to J_{tip} alleviating the stress singularity. Using u_b as before and the strength profile for $h = 0.4$ mm, see Figure 11, that generates a significant enhanced basal resistance over one km distance to the crack tip, calculations show that the reduced pore pressure associated with the presence of a channel removes the stress singularity for $N_c \geq 197$ kPa. At this level of clamping effective stress adjacent to the channel J_{tip} vanishes; the stress field around the crack tip analog becomes singularity free. Based on Table 3 the range of effective pressure we expect next to a marginal channel would be sufficient enough to remove the stress singularity predicted by *Schoof* [2004] associated with the transition between slipping to locked bed and, hence, creates a stable margin configuration. Of course, this model is extremely simplified due to the approximated downstream basal velocity profile taken that should certainly be steeper next to the crack tip analog. However, results here show that enhanced bed resistance next to a marginal channel is an important factor in stabilizing the margin.

Thermal and hydrologic mechanisms contribute together to stabilize a stream margin. The formation of temperate ice generates seepage at the bed and a marginal channel would capture some of the water at the bed. Both mechanisms modify the bed strengthening profile under the stream. One could think of tracking the location of the channel such that J_{tip} reaches zero. In fact, in this context, a natural way of thinking of margin migration would be to find when the bed
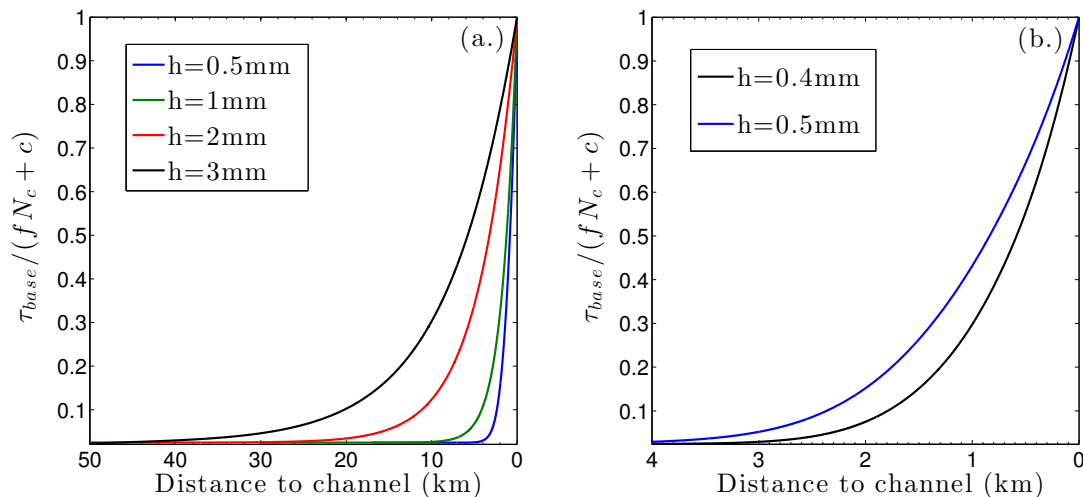
Figure 11. Bed strengthening profile due to the presence of a marginal channel capturing some of the basal meltwater flowing downstream. Simulations are done for Profile WB2 and $N_c = 300$ kPa.

will cease deforming using this procedure. We leave this to future work.

We conjecture that this channelized development and the associated subglacial hydrology at the ice stream margins strengthens the till and locks the ice outboard to the bed, in a manner that contributes to limiting the width of the region of fast-flowing ice. The basal strengthening associated with channelization seems to be a more important factor than the crack blunting associated with the presence of a channel at the crack tip analog in making a singularity free stress field. At least, this hypothesis is consistent with ice streams existing at a widths which correspond, as our results here suggest, to significant internal melt generation.

4. Discussion

4.1. Possible field evidence of temperate ice and channelized bed drainage at margin

Clarke et al. [2000] used a high power radar system to image the entire thickness of the Unicorn (Ridge B1-B2) ice sheet. They made profiles in multiple directions and found numerous linear diffractors near the base of the ice sheet. One special feature that was recognized is the occurrence of diffractors 230 m above the bed, following what they called the "Fishhook", a surface lineation observed in satellite imagery that is parallel to the northern margin of Whillans IS B1 and located at the middle of Unicorn. One possible explanation for these features is that they reflect a zone of wet, temperate ice, that marks the inner boundary of an abandoned shear margin, while the outer boundary is marked by a band of crevasses that used to be the band of arcuate crevasses (now observed at the outer boundary of Dragon margin). This supports the idea already invoked by *Jacobson and Raymond* [1998], *Schoof* [2012] and *Suckale et al.* [2014], that temperate ice is present at the margin over a

substantial fraction of the sheet thickness due to intense shearing.

Clarke et al. [2000] also mentioned that a Caltech group had drilled into the ice at Unicorn approximately 1 km from the outer boundary of the northern margin of Whillans IS B1 (see Figure 6). They reported that, at approximately 56 m above the bed, the drill began encountering abnormal resistance. The penetration rate slowed significantly within layers at 56-49 m, 44-22 m, and 14-0 m above the bed and some fresh scratches were observed on the the metal drill tip once back at the surface. They argue that these observations are strongly suggestive of entrained morainal debris. One of the possible mechanisms of formation of this debris is meltwater processes depositing sediment over a long period of time. We suggest that this morainal debris is a plausible result of marginal channel development at the bed of the abandoned northern shear margin of Whillans IS B1.

Also, a borehole has been made at one shear margin of Kamb IS, the main stream that stopped flowing approximately 150 years ago [*Smith et al.*, 2002]. *Vogel et al.* [2005] drilled to the bottom of the ice sheet at the transition between the active upper part of Kamb IS and its stopped main truck, where the center stream velocity is 25 m.yr^{-1} (see Figure 2). They penetrated a 1.6 m tall water-filled cavity between the bottom of the ice and the bed, a size of the same order of magnitude as our rough estimation of a semicircular channel collecting water from 100 km upstream at Dragon margin. Additionally, videos from the bottom of this borehole showed horizontal advection of small solid particles sinking into the cavity, indicating a still active flow of water within the cavity (the direction of flow was not reported). They estimated that the shear margin reconnected to the basal hydrological system about 60 years ago. They argue that the formation of this 1.6 m tall-water-filled cavity is associated to the re-supply of basal water from areas of basal melting further upstream. This raises the possibility

that the borehole fortuitously encountered a channel of the type that we conjecture. At least, it shows that channelized transport beneath an ice stream margin is a realistic possibility and implies that a source of liquid water must exist near the margin, although we lack data to test with our 1-D model the concept that internal melting is occurring there.

4.2. Effect of surface crevassing and ice advection

Surface crevassing in ice stream margins provides a further link between deformation and internal heating. *Harrison et al.* [1998] used thermistors frozen into boreholes to measure ice temperature as a function of depth at ten locations spanning the margin of Ice Stream B2 (close to profile S1), and found that at a depth of thirty meters the ice temperature in the margin was actually $\sim 10°C$ colder than the neighboring ice in the ridge and stream. This was explained by cold winter air pooling in the heavily crevassing margin. The temperature-depth profiles show that at intermediate depths the ice temperature is no longer influenced by surface crevassing, and below a depth of ~ 150 m the ice temperature within the margin is higher than the temperature in the ridge.

Cold air cools the ice nearest to the surface and hence, strengthening the material. In addition heavily crevassed surface regions will support a lower lateral stress (a cracked material is mechanically softer), forcing the lower portion of the margin to support a larger stress. This focuses shear heating in the lower portion of the margin and alters the expected temperature profile. These processes cannot be properly taken into account properly in our simple modeling. In fact, a discrepancy exists between our simple thermal modeling and the temperature profiles measured near Dragon margin by *Harrison et al.* [1998] in these crevasses. This is a non negligible limitation to the extension of our 1-D model to the particular case of Dragon margin (assuming such similar temperature profiles in the crevasses there). However, a simple adjustment of our 1D thermal model, removing 30 m of ice thickness near the surface, and imposing $T_{atm} = -30°C$, still leads to prediction of a temperate zone with height H' that is 80% of the H' illustrated in Figure 8 and 9. The colder near-surface ice is stronger, hence, more shear heating from forcing it to deform at the observed surface strain rate. Our more elaborate 2-D model in *Suckale et al.* [2014] that approximately matches the measured velocity profile from *Echelmeyer and Harrison* [1999] and temperature profiles from *Harrison et al.* [1998] still suggests the presence of a temperate zone; in this case of 160 m height. This is associated with a water discharge at the bed equivalent to 63% of the one we predict with our simple model; a quantity sufficiently large to be in agreement with the locking process described in this paper according to our sensitivity analysis (see Table 3).

While our model operates at steady state, giving time for the ice to warm because of shear heating at the margin, the temperature profiles measured are accompanied with observations of margin migration. If the migration operates at approximately ten meters per year as predicted by [*Echelmeyer and Harrison*, 1999], the ice would not have enough time to warm up. To our knowledge, *Schoof* [2012] has been the first so far to quantify this process in the approximation of a newtonian fluid by considering a frame that moves with the migrating margin rather than assimilating the horizontal advection to such migration (one can note that an horizontal advection of ~ 2 m.yr^{-1} in both senses is also observed at Dragon margin [*Echelmeyer and Harrison*, 1999]). In *Suckale et al.* [2014], in which the migration is assumed to be equivalent to horizontal motion of ice for the sake of simplicity, the authors find that an advection of meters per year is sufficient to make the temperate region disappear.

Also, a simplified scaling analysis allows to calculate an ice resident time at the margin of approximately $t_{res} = H^2/\alpha_{th} = 10^4$ yr. However, the resident time of the ice at the margin is more likely to be half a century according to *Harrison et al.* [1998]. Therefore it is clear that the steady state approximation is a restriction for our model to match the observed temperature profiles, especially when considering the borehole close to the margin where the non steady state effects are probably the highest. However, if the migration is both outward and inward the resident time of the ice inside the shear margin would become more important and our estimated temperature profiles more realistic. This is consistent with the observation of a complex deformation history that occurred the last few hundred years at Dragon margin [*Clarke et al.*, 2000].

4.3. Margin migration and channelized drainage

In this paper, the thermal regime at the margin is calculated at a steady state. In that, we explicitly assume that margin migration is sufficiently slow to give the time to the ice to warm up due to shear heating. However, one can imagine a scenario in which the margin does slowly grow outward, perhaps in rapid steps of fracturing into the frozen bed, and after each step gets fixed in place. Once fixed in place, as the ice continues to deform, the cold temperature field that we would associate with large horizontal advection would gradually transform towards one with a large zone of temperate ice. That gradual shift of the temperature distribution would presumably show up as changes of the surface velocity profile within the marginal shear zone. In this scenario the migration observed by *Echelmeyer and Harrison* [1999] and *Harrison et al.* [1998] at Dragon margin could perhaps be such a transition and not true migration of the slipping to locked transition.

5. Conclusion

We examine the hypothesis that Western Antarctic Siple Coast ice stream width is set by the development of important internal melting (i.e., development of temperate ice conditions) within the ice sheet at the margins. We first find that the ice deformation-heating work at the margins, when incorporated in a standard 1-D vertical heat transfer analysis [*Zotikov*, 1986], typically predicts temperatures in excess of the melting temperature. We, thus, produce a still 1-D, but more refined thermal model of margins, with a full temperature dependence of ice properties and allowing for a temperate zone adjoining the bed. Using published ice sheet deformation and thickness data, this model predicts that most of active margins of the SCIS are in a state of partial melt, with temperate ice being present over a fraction of the ice height. For the strain rate and sheet thickness given by *Joughin et al.* [2002], we find that, seven of the eight profiles made at the active SCIS are predicted to have temperate ice at the margins. Although the strain rate measured at Bindschadler IS is insufficient to allow a temperate zone to develop, *Scambos et al.* [1994] found, farther downstream, a strain rate at the margins that would melt 55% of the ice sheet thickness according to our model.

Within the temperate zone, the continuous deformation generates internal meltwater, which percolates toward the bed below in veins at triple junctions between ice grains. Using a strain rate profile made at the Dragon margin of Whillans IS B2, we find that the shear heating produces a basal meltwater rate of the order of 10 mm.yr^{-1} over ~ 2 km wide, approximatively the width of the chaotic crevassing zone that appears at this margin's surface. If this seeping meltwater at the margin's bed develops a channelized drainage of Röthlisberger type (R-channel), the accumulated seepage at the estimated rate at Dragon margin, if prevailing over ~ 100 km upstream, is consistent with a

semicircular R-channel of ~ 1 m diameter. We, thus, suggest that ice streams, existing at a width that corresponds to rapid internal melt generation, develop channelized drainage at the ice-till interface of their margins.

We propose a possible related mechanism of the stream's margin formation, which is locking the ice sheet to the bed outboard of this R-channel. Indeed, standard theory argues that the high, nearly lithostatic, pore pressure near the bed of fast-flowing ice is somewhat alleviated within a channel. Our calculations suggest that the Terzaghi effective normal stress, pushing the ice sheet and till together and till particles into one another, can be twenty to sixty times greater at the channel borders than what has been estimated under the rapidly moving central part of the ice stream, and may effectively lock the ice sheet to the bed. This transition between basal slipping under a stream and locked ridges at an ice sheet bed defines an anti-plane shear crack whose surface is the base of the ice sheet beneath the stream and whose tips lie along the shear margins. This crack strongly concentrates stress and strain rate near the shear margins. However, a crack ending in a channel, such as we predict at the margins, has greatly diminished stress and strain rate concentration, and the high Terzaghi effective normal stress just outside the channel, which increases basal shear resistance, contributes toward resisting continued expansion of the slipping zone. This may lock the ice sheet to the bed outboard of the marginal channels and naturally form an ice stream shear margin, as a limit to the fast-flowing ice.

Notation

a surface accumulation rate of ice, m.s^{-1}.

A temperature-dependent creep parameter, s^{-1}.Pa^{-3}.

A_{melt} ice creep parameter at the melting point, s^{-1}.Pa^{-3}.

A_c channel cross-sectional area, m^2.

α_{th} thermal diffusivity of ice, m^2.s^{-1}.

c till cohesion, Pa.

C_i ice specific heat, J.kg^{-1}.K^{-1}.

D channel diameter, m.

f till friction coefficient, [1].

f_{dw} Darcy-Weisbach friction coefficient at the channel's wall, [1].

$\dot{\gamma}_{lat}$ lateral "engineering" shear strain rate, s^{-1}.

g acceleration due to gravity, m.s^{-2}.

G_{geo} geothermal heat flux, W.m^{-2}.

G_{ice} heat lost by ice conduction at the base of the ice sheet, W.m^{-2}.

H ice sheet thickness, m.

H' temperate height of ice, m.

k Nikuradse channel wall-roughness amplitude, m.

k_{ice} ice permeability, m^2.

K ice thermal conductivity, W.m^{-1}.K^{-1}.

L_f latent heat per unit mass, J.kg^{-1}.

$\dot{m}$ melt rate per unit of volume, kg.s^{-1}.m^{-3}.

μ_w dynamic viscosity of water, Pa.s.

n_m Gaukler-Manning-Strickler roughness coefficient, s.m$^{-1/3}$.

N Effective pressure, Pa.

N_c Effective pressure adjacent to the marginal channel, Pa.

p water pore pressure, Pa.

p_{ch} water pore pressure inside the marginal channel, Pa.

Pe   Péclet number, [1].

q_w vertical water Darcy flux, m.s^{-1}.

q_{temp} vertical downward water Darcy flux at the bed, m.s^{-1}.

Q_w water discharge rate in the marginal channel, m^3.s^{-1}.

ρ_w density of water, kg.m^{-3}.

ρ_{ice} density of ice, kg.m^{-3}.

R_h channel hydraulic radius, m.

S absolute value of the downstream surface slope, [1].

σ_0 ice overburden pressure, Pa.

$T(z)$ vertical temperature profile, K.

T_{wf} hydraulic transmissivity of the water film at the ice-till interface, m^2.s^{-1}.

T_{melt} basal melting temperature of ice, K.

T_{atm} atmospheric temperature, K.

t time, s.

t_0 time scale used in the thermal boundary layer at the base of the ice sheet, s.

τ_{lat} local lateral shear stress parallel to the downslope direction, Pa.

$\bar{\tau}_{lat}$ average of the lateral shear stress over the ice thickness, Pa.

τ_{grav} gravitational driving stress, Pa.

τ_{base} local basal shear stress, Pa.

$\bar{\tau}_{base}$ width-average basal shear stress, Pa.

τ_{wall} wall stress acting over the channel wetted perimeter, Pa.

u_b downstream basal velocity, m.s^{-1}.

U average velocity inside the channel, m.s^{-1}.

x downstream cartesian coordinate, m.

y cross-slope cartesian coordinate starting at the stream center, m.

$\hat{y}$ cross-slope cartesian coordinate starting at the channel, m.

z cartesian coordinate measured perpendicularly to the bed, m.

v_m basal melt rate, m.s^{-1}.

w upward velocity measured perpendicularly to the bed, m.s^{-1}.

W ice stream width, m.

Φ volumetric rate of internal heat production, W.m^{-3}

References

Bamber, J. L., R. E. M. Riva, B. L. A. Vermeersen, and A. M. Le Brocq, Reassessment of the Potential Sea-Level Rise from a

Collapse of the West Antarctic Ice Sheet, *Science*, *324*(5929), 901–903, doi:10.1126/science.1169335, 2009.

Barenblatt, G. I., On equilibrum cracks formed in brittle fracture, *Appl. Math. Mech.*, *23*(3), 1959.

Beem, L. H., K. C. Jezek, and C. Van Der Veen, Basal melt rates beneath Whillans Ice Stream, West Antarctica, *J. Glaciol.*, *56*(198), 647–654, 2010.

Ben Amar, M., and J. Rice, Exacts results with the J-integral applied to free-boundary flows, *J. Fluid Mech.*, *461*, 321–341, 2002.

Bilby, B., and J. Eshelby, Dislocations and the Theory of Fracture, in *Fracture: An Advanced Treatise: Vol. 2, Mathematical Fundamentals*, edited by H. Liebowitz, pp. 99–182, Academic Press, N.Y., 1968.

Bilby, B. A., A. H. Cottrell, and K. H. Swinden, The spread of plastic yield from a notch, *Proc. R. Soc. Lond. A.*, *272*(1350), 304–314, doi:10.1098/rspa.1963.0055, 1963.

Cherepanov, G., Cracks in solids, *International Journal of Solids and Structures*, *4*(8), 811–831, 1968.

Clarke, G. K. C., Hydraulics of subglacial outburst floods: new insights from the spring-hutter formulation, *J. Glaciol.*, *49*(165), 299–313, 2003.

Clarke, T. S., C. Liu, N. E. Lord, and C. R. Bentley, Evidence for a recently abandoned shear margin adjacent to ice stream B2, Antarctica, from ice-penetrating radar measurements, *J. Geophys. Res.*, *105*(B6), 2000.

Creyts, T. T., and C. G. Schoof, Drainage through subglacial water sheets, *J. Geophys. Res.*, *114*(F04008), doi:10.1029/2008JF001215, 2009.

Cuffey, K., and W. Paterson, *The Physics of Glaciers (Fourth Edition)*, ISBN 9780123694614, Elsevier, 2010.

Dugdale, D., Yielding of steel sheets containing slits, *J. Mech. Phys. Solids*, *8*(2), 100–104, 1960.

Echelmeyer, K., and W. Harrison, Ongoing margin migration of Ice Stream B, Antarctica, *J. Glaciol.*, *45*(150), 361–369, 1999.

Echelmeyer, K., W. Harrison, C. Larsen, and J. Mitchell, The role of the margins in the dynamics of an active ice stream, *J. Glaciol.*, *40*(136), 527–538, 1994.

Engelhardt, H., Ice temperature and high geothermal flux at siple dome, west antarctica, from borehole measurements, *J. Glaciol.*, *50*(169), 251–256, doi:10.3189/172756504781830105, 2004.

Fricker, H. A., and T. Scambos, Connected subglacial lake activity on lower Mercer and Whillans Ice Streams, West Antarctica, 20032008, *J. Glaciol.*, *55*(190), 303–315, 2009.

Fricker, H. A., T. Scambos, S. Carter, C. Davis, T. Haran, and I. Joughin, Synthesizing multiple remote-sensing techniques for subglacial hydrologic mapping: application to a lake system beneath MacAyeal Ice Stream, West Antarctica, *J. Glaciol.*, *56*(196), 187–199, doi:10.3189/002214310791968557, 2010.

Gioia, G., and P. Chakraborty, Turbulent Friction in Rough Pipes and the Energy Spectrum of the Phenomenological Theory, *Physical Review Letters*, *96*(044502), 2006.

Giovinetto, M., and H. Zwally, Spatial distribution of net surface accumulation on the antarctic ice sheet, *Ann. Glaciol.*, *31*, 2000.

Goldman, N., and J. Hutchinson, Fully plastic crack problems: The center-cracked strip under plane strain, *International Journal of Solids and Structures*, *11*(5), 575–591, 1975.

Harrison, W., K. A. Echelmeyer, and C. Larsen, Measurement of temperature in a margin of Ice Stream B, Antarctica : implications for margin migration and lateral drag, *J. Glaciol.*, *44*(148), 1998.

Hewitt, I. J., Modelling distributed and channelized subglacial drainage: the spacing of channels, *J. Glaciol.*, *57*(202), 302–314, doi:10.3189/002214311796405951, 2011.

Hooke, R. L., *Principles of Glacier Mechanics*, Second ed., Cambridge University Press, 2005.

Jackson, M., and B. Kamb, The marginal shear stress of Ice Stream B, West Antarctica, *J. Glaciol.*, *43*(145), 415–426, 1997.

Jacobson, H., and C. Raymond, Thermal effects on the location of ice stream margins, *J. Geophys. Res.*, *103*(B6), 111–122, 1998.

Jordan, R., and J. Stark, Capillary Tension in Rotting Ice Laters, *Tech. rep.*, Technical Report ERDC/CRREL TR-01-13. US Army Corps of Engineers, Cold Regions Research and Engineering Laboratory, 2001.

Joughin, I., S. Tulaczyk, R. Bindschadler, and S. F. Price, Changes in West Antarctic Ice Stream velocities: Observation and analysis, *J. Geophys. Res.*, *107*(B11), doi:10.1029/2001JB001029, 2002.

Joughin, I., S. Tulaczyk, and H. Engelhardt, Basal melt beneath Whillans Ice Stream and Ice Streams A and C, West Antarctica, *Ann. Glaciol.*, *36*, 257–262, doi:10.3189/172756403781816130, 2003.

Joughin, I., D. R. MacAyeal, and S. Tulaczyk, Basal shear stress of the Ross ice streams from control method inversions, *J. Geophys. Res.*, *109*(B9), doi:10.1029/2003JB002960, 2004a.

Joughin, I., S. Tulaczyk, D. R. MacAyeal, and H. Engelhardt, Melting and freezing beneath the Ross ice streams, Antarctica, *J. Glaciol.*, *50*(168), 96–108, doi:10.3189/172756504781830295, 2004b.

Joughin, I., et al., Continued deceleration of Whillans Ice Stream, West Antarctica, *Geophys. Res. Lett.*, *32*(22), L22,501, doi:10.1029/2005GL024319, 2005.

Kamb, B., Basal zone of the West Antarctic Ice Streams and its role in lubrication of their rapid motion, in *The West Antarctic Ice Sheet: Behavior and Environment*, vol. 77, edited by R. B. Alley and R. A. Bindschadler, pp. 157–199, AGU, Washington, DC, doi:10.1029/AR077p0157, 2001.

Kubo, S., K. Ohji, and K. Ogura, Analysis of creep crack-propagation on the basis of the plastic singular stress-field, *Engineering Fracture Mechanics*, *11*(2), 315–329, 1979.

Kyrke-Smith, T., R. Katz, and A. Fowler, Subglacial hydrology and the formation of ice streams, *Proc. Roy. Soc. A*, *470*(2161), doi:10.1098/rspa.2013.0494, 2014.

Landes, J., and J. Begley, A fracture mechanics approach to creep crack growth, in *Mechanics of Crack Growth*, pp. 128–148, Amer. Soc. for Testing and Materials (ASTM), Special Technical Publication (STP) 590, Philadelphia, 1976.

Le Brocq, A., A. Payne, M. Siegert, and R. Alley, A subglacial water-flow model for West Antarctica, *J. Glaciol.*, *55*(193), 879–888, doi:10.3189/002214309790152564, 2009.

Lythe, M. B., and D. G. Vaughan, Bedmap: A new ice thickness and subglacial topographic model of Antarctica, *J. Geophys. Res.*, *106*(B6), 11,335–11,351, doi:10.1029/2000JB900449, 2001.

Maule, C. F., M. E. Purucker, N. Olsen, and K. Mosegaard, Heat flux anomalies in antarctica revealed by satellite magnetic data, *Science*, *309*(5733), 464–467, doi:10.1126/science.1106888, 2005.

McMeeking, R., and R. Johnson, On the mechanics of surging glaciers, *Journal of Glaciology*, *32*(110), 120–132, 1986.

Nye, B. F., and F. C. Frank, Hydrology of the intergranular veins in a temperate glacier, *J. Glaciol.*, 1973.

Nye, J., The flow law of ice from measurements in glacier tunnels, laboratory experi- ments and the jungfraufirn borehole experiment, *Proc. R. Soc. Lond. Ser. A 219*, pp. 477–489, 1953.

Nye, J., Water flow in glaciers: jökulhlaups, tunnels and veins, *J. Glaciol.*, *17*(76), 181–207, 1976.

Nye, J., The geometry of water veins and nodes in polycrystalline ice, *J. Glaciol.*, *35*, 17–22, 1989.

Perol, T., J. D. Platt, J. R. Rice, and J. Suckale, Stressing, hydraulic and locking processes at ice stream margins, abstract C11B-0677 presented at 2012 Fall Meeting, AGU, San Francisco, Calif., 5-9 Dec., 2012.

Rathbun, A., C.Marone, R. Alley, and S. Anandakrishnan, Laboratory study of the frictional rheology of sheared till, *J. Geophys. Res.*, *113*(F02020), doi:10.1029/2007JF000815, 2008.

Raymond, C., K. Echelmeyer, I. Whillans, and C. Doake, Ice stream shear margins, in *The West Antarctic Ice Sheet: Behavior and Environment*, vol. 77, pp. 137–55, American Geophysical Union, Antarctic Research Series, 2001.

Rice, J., A path independent integral and the approximate analysis of strain concentration by notches and cracks, *Journal of Applied Mechanics*, *35*, 379–386, 1968a.

Rice, J., Mathematical analysis in the mechanics of fracture, in *Fracture: An Advanced Treatise: Vol. 2, Mathematical Fundamentals*, edited by H. Liebowitz, pp. 191–311, Academic Press, N.Y., 1968b.

Röthlisberger, H., Water pressure in intra- and subglacial channels, *J. Glaciol.*, *11*(62), 177–203, 1972.

Sayag, R., and E. Tziperman, Spatiotemporal dynamics of ice streams due to a triple-valued sliding law, *J. Fluid Mech.*, *640*, 483, 2009.

Scambos, T., K. Echelmeyer, M. Fahnestock, and R. Bind-schadler, Develoment of enhanced ice flow at the southern margin of Ice Stream D, Antarctica, *Ann. Glaciol.*, *20*, 313–318, 1994.

Schoof, C., On the mechanics of ice-stream shear margins, *J. Glaciol.*, *50*(169), 208–218, doi:10.3189/172756504781830024, 2004.

Schoof, C., Ice-sheet acceleration driven by melt supply variability, *Nature*, *468*, doi:10.1038/nature09618, 2010.

Schoof, C., Thermally-driven migration of ice stream shear margins, *J. Fluid Mech.*, *712*, 2012.

Shabtaie, S., and C. Bentley, West Antarctic Ice Streams Draining into the Ross Ice Shelf: Configuration and Mass Balance, *J. Geophys. Res.*, *92*, 1311–1336, 1987.

Smith, B., N. Lord, and C. Bentley, Crevasse ages on the northern margin of Ice Stream C, West Antarctica, *Ann. Glaciol.*, *34*(1), 209–216, doi:10.3189/172756402781817932, 2002.

Spikes, V. B., G. S. Hamilton, S. A. Arcone, S. Kaspari, and P. A. Mayewski, Variability in accumulation rates from GPR profiling on the West Antarctic plateau, *Ann. Glaciol.*, *39*, 2004.

Suckale, J., J. D. Platt, T. Perol, and J. R. Rice, Deformation-induced melting in the margins of the West Antarctic ice streams, *J. Geophys. Res. Earth Surf.*, *119*, doi:10.1002/2013JF003008, 2014.

Tulaczyk, S., W. B. Kamb, and H. Engelhardt, Basal mechanics of Ice Stream B, West Antarctica 1. till mechanics, *J. Geophys. Res.*, *105*(B1), 463–481, doi:10.1029/1999JB900329, 2000.

Van Der Veen, C., and I. Whillans, Model experiments on the evolution and stability of ice streams, *Ann. Glaciol.*, *23*, 129–137, 1996.

Vaughan, D. G., and J. R. Spouge, Risk Estimation of Collapse of the West Antarctic Ice Sheet, *Climatic Change*, *52*, 65–91, doi:10.1023/A:1013038920600, 2002.

Vogel, S., The basal regime of the West-Antarctic Ice Sheet. interaction of subglacial geology with ice dynamics, Ph.D. thesis, University of California Santa Cruz, 2004.

Vogel, S. W., S. Tulaczyk, B. Kamb, H. Engelhardt, F. D. Carsey, A. E. Behar, A. L. Lane, and I. Joughin, Subglacial conditions during and after stoppage of an Antarctic Ice Stream: Is reactivation imminent?, *Geophys. Res. Lett.*, *32*, doi:10.1029/2005GL022563, 2005.

Weertman, J., General theory of water flow at base of a glacier or ice sheet, in *Reviews of Geophysics and Space physics*, vol. 10, pp. 287—333, American Geophysical Union, doi: doi:10.1029/RG010i001p00287, 1972.

Whillans, I., and C. Van Der Veen, New and improved determinations of velocity of Ice Streams B and C, West Antarctica, *J. Glaciol.*, 1993.

Whillans, I., and C. Van der Veen, The role of lateral drag in the dynamics of Ice Stream B, Antarctica, *J. Glaciol.*, *43*(144), 231–237, 1997.

Whillans, I., C. Bentley, and C. Van Der Veen, Ice streams B and C, in *The West Antarctic Ice Sheet: Behavior and Environment*, *Antarct. Res. Ser.*, vol. 77, edited by R. Alley and R. A. Bindschadler, pp. 257–281, AGU, Washington, D.C., 2001.

Zotikov, I., *The Thermophysics Of Glaciers*, D. Reidel, Mass, 1986.

Thibaut Perol, School of Engineering and Applied Sciences, Harvard University, 327 Pierce Hall, 29 Oxford Street, Cambridge, MA 02138, USA. (tperol@seas.harvard.edu)

James R. Rice, Department of Earth and Planetary Sciences and School of Engineering and Applied Sciences, Harvard University, 224 Pierce Hall, 29 Oxford Street, Cambridge, MA 02138, USA. (rice@seas.harvard.edu)

Appendix A: Analytical solution of the 1-D conduction-advection model with internal heating

To solve

$$\alpha_{th}\frac{\mathrm{d}^2T}{\mathrm{d}z^2} + \frac{az}{H}\frac{\mathrm{d}T}{\mathrm{d}z} + \frac{\tau_{lat}\dot{\gamma}_{lat}}{\rho_{ice}C_i} = 0, \quad (A1)$$

let us define $G = (\mathrm{d}T/\mathrm{d}z)$, $\eta = (z/H)^2$, $S = \tau_{lat}\dot{\gamma}_{lat}$ and $\mathrm{Pe} = aH/\alpha$ the Péclet number. Then, the previous equation reduces to,

$$2\alpha_{th}\frac{\mathrm{d}G}{\mathrm{d}\eta} + aHG = -\frac{SH}{\rho_{ice}C}\frac{1}{\sqrt{\eta}}, \quad (A2)$$

and integration gives,

$$\begin{aligned}G &= G_0\exp(-\mathrm{Pe}z^2/2H^2)\\&\quad -\frac{S}{K}\int_0^z\exp\left[-\mathrm{Pe}(z^2-\tilde{z}^2)/2H^2\right]\mathrm{d}\tilde{z},\end{aligned} \quad (A3)$$

with $G_0 = (\mathrm{d}T/\mathrm{d}z)_{z=0}$. We integrate the latter relation using $T(z=0) = T_{melt}$ and find

$$\begin{aligned}T(z) &= T_{melt} + \sqrt{\frac{\pi}{2\mathrm{Pe}}}HG_o\,\mathrm{erf}\left(\frac{\sqrt{\mathrm{Pe}/2}\,z}{H}\right)\\&\quad -\frac{S}{K_{avg}}\int_0^z\int_0^{\hat{z}}\exp\left[\mathrm{Pe}(\tilde{z}^2-\hat{z}^2)/2H^2\right]\mathrm{d}\tilde{z}\mathrm{d}\hat{z}.\end{aligned} \quad (A4)$$

Using polar coordinates in the integrations in the $z, \tilde{z}$ plane, the analytical temperature distribution along the z-axis is

$$\begin{aligned}T(z) &= T_{melt} + \sqrt{\frac{\pi}{2\mathrm{Pe}}}HG_o\,\mathrm{erf}\left(\frac{\sqrt{\mathrm{Pe}/2}\,z}{H}\right)\\&\quad -\frac{SH^2}{K_{avg}\mathrm{Pe}}\int_0^{\pi/4}\frac{1-\exp\left(-\frac{\mathrm{Pe}\cos(2\theta)}{2\cos^2(\theta)}\frac{z^2}{H^2}\right)}{\cos(2\theta)}\mathrm{d}\theta.\end{aligned} \quad (A5)$$

Rewriting the latter integral, the temperature profile along the z-axis is

$$\begin{aligned}T(z) &= T_{melt} + \sqrt{\frac{\pi}{2\mathrm{Pe}}}HG_0\,\mathrm{erf}\left(\sqrt{\mathrm{Pe}/2}\,\frac{z}{H}\right)\\&\quad -\frac{\tau_{lat}\dot{\gamma}_{lat}H^2}{K_{avg}\mathrm{Pe}}\int_0^1\frac{1-\exp\left(-\lambda\mathrm{Pe}z^2/2H^2\right)}{2\lambda\sqrt{1-\lambda}}\mathrm{d}\lambda\end{aligned} \quad (A6)$$

and G_0 is found matching the second boundary condition $T(z=H) = T_{atm}$,

$$\begin{aligned}G_0 &= \frac{2\sqrt{\mathrm{Pe}/2}}{\sqrt{\pi}H\,\mathrm{erf}\left(\sqrt{\mathrm{Pe}/2}\right)}\left(T_{atm}-T_{melt}\right.\\&\quad \left.+\frac{\tau_{lat}\dot{\gamma}_{lat}H^2}{K_{avg}\mathrm{Pe}}\int_0^1\frac{1-\exp\left(-\lambda\mathrm{Pe}/2\right)}{2\lambda\sqrt{1-\lambda}}\mathrm{d}\lambda\right)\end{aligned} \quad (A7)$$

Appendix B: Hydrological strengthening of the bed next to a marginal channel

Here we derive the pore pressure profile at the ice-till interface considering a thin water film of thickness h, expected to be of mm scale. The till is considered as a Coulomb-Plastic material. The coordinates x and z are the same than in the rest of the paper but to simplify the notations we now use $\hat{y}$ transverse to the flow with its origin at the channel and negative under the ice stream ($\hat{y} = y - W/2$ so that $\hat{y} = -W/2$ at the stream center). The hat on the coordinates show the distinction with the coordinates system used for thermal modeling.

B1. Governing equations

Heat Balance: The heat balance at the ice-till interface is

$$G_{geo} - G_{ice} + \tau_{base}\, u_b = \rho_{ice}Lv_m, \qquad (B1)$$

where G_{geo} is the geothermal heat flux and G_{ice} is the heat flux through the ice at the base of the ice sheet and u_b is the ice velocity at the base. The other parameters are as defined before (also see Notations list). At the base of the ice sheet the major velocity component is in the downstream direction and it is reasonable to assume frictional heating as being only $\tau_{base}u_b$. Moreover, we ignore the heat generated by dissipation in meltwater seepage shown to be negligible in the heat equation by scaling arguments (see for example *Kyrke-Smith et al.* [2014]).

In a thermal boundary layer at the bottom of the ice sheet the transient 1D heat equation (2) is

$$\frac{\partial T}{\partial t} = \frac{K}{\rho_{ice}C_i} \frac{\partial^2 T}{\partial z^2}. \qquad (B2)$$

The equation when solved in a semi infinite space with $T = T_{melt}$ at the ice till interface and T_{atm} at infinity in z (since H is much larger than the size of the boundary layer) admits an error function as a similarity solution and the derived flux is

$$G_{ice} = (T_{melt} - T_{atm}) \left(\frac{\rho_{ice}C_iK}{\pi\, t_0} \right)^{1/2} \qquad (B3)$$

where t is replaced by a time scale t_0 over which the stream has evolved; t_0 is given in the text in subsection 3.4.2. This dominant balance becomes less accurate close to the channel where temperate ice is present over some height adjacent to the bed. However, the width of the melted margin is small compare to the width of the stream and hence, it seems sufficiently accurate for a great domain under the stream.

Water mass conservation: The water flow through the system till-water film is balanced by basal melting that occurs and the seepage from temperate ice q_{temp} (in m.s^{-1}),

$$\rho_w \nabla \cdot \mathbf{Q} = \rho_{ice}v_m + \rho_w q_{temp}. \qquad (B4)$$

q_{temp} is an input parameter based on the thermal modeling. $\mathbf{Q}$ is the flow rate vector in m^2/s.

Porous flow: The hydraulic potential ψ at the ice-till interface is simply $p + \rho_w gz$ where p is the local absolute pore pressure and z is the elevation (e.g., relative to mean see level) so that

$$\psi = p_{atm} + \rho_i gH + \rho_w gz - N \qquad (B5)$$

where p_{atm} is the atmospheric pressure that is negligible and $N = p_{atm} + \rho_i gH - p$ is the effective pressure. The hydraulic head is $h = \psi/(\rho_w g)$.

Using Darcy's law, $\mathbf{q}$, the Darcy velocity vector in m/s, is linearly related to the the hydraulic head via the hydraulic conductivity. We use Dupuit's approximation and thus define the flow rate through the system till-water film as

$$\mathbf{Q} = \int_{-h}^{0} \mathbf{q}(x, \hat{y})\mathrm{d}z = -\frac{T_{wf}}{\rho_w g}\nabla\psi. \qquad (B6)$$

where T_{wf} is the hydraulic transmissivity of the water film. Using a till hydraulic conductivity of 10^{-10} m/s [*Tulaczyk et al.*, 2000] and a till thickness of order of 1 m [*Tulaczyk et al.*, 2000; *Kamb*, 2001; *Whillans et al.*, 2001], the till transmissivity is 10^{-10} m^2/s and, therefore, we can neglect its contribution to the water flow. Assuming a local Poiseuille flow in the water film,

$$\int_{-h}^{0} \mathbf{q}(x, \hat{y})\mathrm{d}z = -\frac{h^3}{12\mu}\nabla\psi. \qquad (B7)$$

From this we can invert a water film transmissivity $T_{wf} = (h^3\rho_w g)/(12\mu_w)$ that is 4.5×10^{-4} m^2/s for a water film thickness of 1 mm.

Mechanical coupling of the till and the ice: The ice is flowing directly over the till. The resistance to the flow occurs at the contact between ice and clasts of till and hence, we have

$$\tau_{base} = fN + c \qquad (B8)$$

where f is the friction coefficient and c the cohesion coefficient.

Finally, using the previous relation together with equation (B1), (B3), (B4) and (B6), assuming that the ice surface has a constant uniform downstream slope and no transverse slope and that the downstream pressure gradient is constant, $\partial^2 N/\partial x^2 = 0$, we obtain

$$G_{geo} - (T_{melt} - T_{atm}) \left(\frac{\rho_{ice}C_iK}{\pi\, t_0} \right)^{1/2} \qquad (B9)$$

$$+ (fN + c)u_b + \rho_w Lq_{temp} = \frac{T_{wf}L}{g} \frac{\partial^2 N}{\partial \hat{y}^2}$$

Now inserting $\tau_{base} = fN + c$ we can solve for the strength profile away from the channel (see equation 34 in the subsection 3.4)